EHD2 regulates plasma membrane integrity and downstream insulin receptor signalling events

EHD2: membrane integrity and insulin signalling

Mathis Neuhaus[1], Claes Fryklund[1], Holly Taylor[2], Andrea Borreguero-Muñoz[1], Franziska Kopietz[1], Hamidreza Ardalani[3], Oksana Rogova[3], Laura Stirrat[2], Shaun K. Bremner[2], Peter Spégel[3], Nia J. Bryant[4], Gwyn W. Gould[2], Karin G. Stenkula[1]

[1]Department of Experimental Medical Science, Lund University, Sweden
[2]Strathclyde Institute for Pharmacy and Biomedical Sciences, University of Strathclyde, Glasgow G4 0RE, UK
[3]Department of Chemistry, Centre for Analysis and Synthesis, Lund University, Sweden
[4]Department of Biology and York Biomedical Research Institute, University of York, York YO10 4HJ, UK

Corresponding author: Mathis Neuhaus, e-mail: mathis.neuhaus@med.lu.se, ORCID: 0000-0003-1091-4757+46-46-2220878, Lund University, BMC, C11, 22184 Lund, SWEDEN

Keywords

EHD2, caveolae, insulin receptor, GLUT4, adipocytes, plasma membrane

Summary

EH domain-containing protein 2 (EHD2) is one of the highest upregulated genes at the early stage of adipose tissue expansion. Using knockout mice and cell models, we show that EHD2 plays a key role in proximal and distal insulin signalling, and is important for maintenance of the plasma membrane milieu and insulin receptor stability in adipocytes.

Abstract

Adipocyte dysfunction is a crucial driver of insulin resistance and type 2 diabetes. We identified EH domain-containing protein 2 (EHD2) as one of the most highly upregulated genes at the early stage of adipose tissue expansion. EHD2 is a dynamin-related ATPase influencing several cellular processes, including membrane recycling, caveolae dynamics and lipid metabolism. Here, we investigated the role of EHD2 in adipocyte insulin signalling and glucose transport. Using C57BL6/N EHD2 knockout mice under short-term high-fat diet conditions and 3T3-L1 adipocytes we demonstrate that EHD2 deficiency is associated with deterioration of insulin signal transduction and impaired insulin-stimulated GLUT4 translocation. Furthermore, we show that lack of EHD2 is linked with altered plasma membrane lipid and protein composition, reduced insulin receptor expression, and diminished insulin-dependent SNARE protein complex formation. In conclusion, these data highlight the importance of EHD2 for the integrity of the plasma membrane milieu, insulin receptor stability, and downstream insulin receptor signalling events, involved in glucose uptake and ultimately underscore its role in insulin resistance and obesity.

Abbreviations

AS160	Akt substrate of 160 kD
CAV1	Caveolin-1
EHD2	EH domain-containing protein 2
KD	Knockdown
KO	Knockout
GSV	GLUT4 storage vesicles
GLUT4	Glucose transporter 4
HFD	High-fat diet
HSP90	Heat shock protein 90
IRβ	Insulin receptor beta
IRS-1	Insulin receptor substrate-1
NKA	Na^+/K^+-ATPase
PKB (Akt)	Protein kinase B
PLA	Proximity ligation assay
PM	Plasma membrane
SNARE	Soluble N-ethylmaleimide-sensitive factor-attachment protein receptors

Introduction

Obesity is one of the most serious challenges for global health in the 21st century. In the United States the obesity prevalence rate has increased from 30.5% to 42.4% the last 20 years, and excess weight is a well-established risk factor for numerous diseases, including insulin resistance and type 2 diabetes. Overweight and obesity are characterized by impaired adipocyte function, involving reduced insulin sensitivity, lowered glucose uptake and impaired lipid storage capacity, which negatively influences whole-body glucose homeostasis (Acosta et al., 2016).

Caveolae are omega-shaped plasma membrane invaginations with a broad range of functions, e.g., the orchestration of lipid transport (Pohl et al., 2005), facilitation of transmembrane signalling (Cohen et al., 2003), and stabilization of the insulin receptor (Gustavsson et al., 1999). Approximately one-third of the adipocyte cell surface area is occupied by caveolae (Thorn et al., 2003), and mounting evidence implies that caveolae capture a critical function in maintaining proper insulin signalling in adipocytes (reviewed in (Stralfors, 2012)). Ablation or mutation of the caveolin core proteins, namely cavins and caveolins, leads to impaired insulin signalling in adipose tissue, hyperinsulinemia and insulin resistance (Gustavsson et al., 1999, Cohen et al., 2003), and lipodystrophy in both rodent models (Razani et al., 2002, Liu et al., 2008) and humans (Cao et al., 2008, Kim et al., 2008). Further, Cohen *et al.* reported an increased proteasomal degradation of insulin receptor beta (IRβ) and insulin receptor substrate (IRS-1) in caveolin-1 (CAV1) deficient mice (Cohen et al., 2003). Consequently, caveolae structures potentially stabilize the insulin receptor, govern insulin signal transduction and exert significant effects on insulin-dependent processes in adipocytes. Consistent with this, caveolae-mediated endocytosis of the insulin receptor drives dephosphorylation of the autophosphorylated insulin receptor and thus ensures proper insulin signalling (Fagerholm et al., 2009, Chen et al., 2019). However, the exact interplay of caveolae and insulin signalling remains to be elucidated. One possible way caveolae might influence insulin signalling could be related to the unique lipid environment of caveolae structures which are enriched in cholesterol, sphingomyelin, and phosphatidylethanolamine; indeed previous studies indicate that both the activity and stability of IRβ are affected by membrane lipid alterations (Vainio et al., 2002, Ginsberg et al., 1981).

EH domain-containing protein 2 (EHD2) is a dynamin-related ATPase (Daumke et al., 2007) that oligomerizes at the neck of caveolae where it is proposed to stabilize caveolae at the plasma membrane through cytoskeletal anchoring (Moren et al., 2012, Stoeber et al., 2012).

This was illustrated by EHD2 knockdown (KD) which caused increased caveolae detachment (Matthaeus et al., 2020)(Moren et al., 2012). Following a short-term high-fat diet (HFD) feeding intervention, we discovered EHD2 as one of the most differentially expressed genes in adipose tissue (Hansson et al., 2018). In recent studies, we and others have confirmed a role for EHD2 in lipid handling using a global EHD2 knockout (EHD2 KO) C57Bl6/N mouse model, which displayed altered lipid metabolism (Matthaeus et al., 2020, Fryklund et al., 2021), impaired lipolysis and diminished insulin-mediated inhibition of lipolysis in primary adipocytes (Fryklund et al., 2021). Interestingly it was previously shown that antibody-induced EHD2 inhibition reduced insulin-stimulated GLUT4 translocation (Park et al., 2004), emphasizing a role of EHD2 for insulin-dependent cellular events. A key mechanism regulating the insulin-stimulated delivery of intracellular GLUT4 sortage vesicles (GSV) to the plasma membrane is the assembly of Soluble N-ethylmaleimide-sensitive factor-attachment protein receptor (SNARE) protein complexes (Bryant et al., 2002). Both the structure of individual SNARE proteins (Fezoua-Boubegtiten et al., 2019, Lakomek et al., 2019, Wang et al., 2020, Saito et al., 2012), their localization (Chamberlain et al., 2001, Salaun et al., 2005, Lang et al., 2001) and their assembly has been shown to depend on the membrane lipid environment (Chamberlain and Gould, 2002, Schnitzer et al., 1995). Accordingly, due to the exceptionally high abundance in adipocytes and the unique lipid composition of caveolae, it could be postulated that SNARE function might be affected by caveolae intergrity. However, to the best of our knowledge, the impact of EHD2 deficiency on insulin signalling and SNARE protein complex formation has not been elucidated.

Therefore, we set out to examine the effects of EHD2 deficiency on insulin signalling, glucose uptake, and plasma membrane lipid composition using primary adipocytes isolated from C57BL6/N EHD2 KO mice. In addition, by siRNA-induced EHD2 knockdown (KD) in cultured 3T3-L1 adipocytes, we examined the role of EHD2 in SNARE complex assembly and caveolin-1- IRβ interactions. We demonstrate that EHD2 deficiency negatively influences IRβ stability and downstream events, including SNARE protein complex formation, GLUT4 dynamics and glucose uptake and posit that EHD2 plays a key role in the organisation and integrity of insulin signalling and plasma membrane composition.

Methods

Material

Insulin receptor substrate 1 (IRS-1) (#06-248, RRID:AB_2127890, Merck Millipore, Billerica, USA), phospho IRS-1 Y612 (#44-816G, RRID:AB_2533768, Life Technologies, Carlsbad, USA), AS160 Akt substrate of 160 kDa (#07-741, RRID:AB_492639, EMD Millipore, Darmstadt, Germany). Protein kinase B (Akt) (#4691, RRID:AB_915783), phospho Akt S473 (#4060S, RRID:AB_2315049), phospho AS160 Thr642 (#4288S, RRID:AB_10545274), Glyceraldehyde 3-phosphate dehydrogenase (GAPDH) (RRID:AB_2536381, Thermo Fisher Scientific Cat, Massachusetts, USA) and Sodium-potassium ATPase (Na^+/K^+-ATPase) (#96124, RRID:AB_2800256) were from Cell Signalling (Cambridge, UK). Caveolin-1 (CAV1) (#610407, RRID:AB_397789) and Heat shock protein (HSP) 90 antibody (#610418, RRID:AB_397798) were from BD Biosciences (Franklin Lakes, US). Cavin 1 (#ab48824, RRID:AB_882224) and EHD2 (Abcam Cat# ab154784, RRID:AB_2927498)) were from Abcam (Cambridge, UK). Mammalian uncoordinated-18c (Munc18c) (#116 202, RRID:AB_2619785), Syntaxin 4 (Sx4) (#110 042, RRID:AB_887853), vesicle associated membrane protein 2 (VAMP2) (#104 403, RRID:AB_2864782), Synaptosome Associated Protein 23 (SNAP23) (#111 213, RRID:AB_10805651), and Syntaxin 16 (Sx16) (#110 162, RRID:AB_887799) were all from Synaptic Systems (Coventry, UK). GLUT4 used for 3T3-L1 analysis (#PA1-1065 RRID:AB_2191454, Thermo Fisher Scientific Cat, Massachusetts, USA), insulin regulated aminopeptidase (IRAP) (#sc-365300, RRID:AB_10844333) and Insulin receptor beta (IRβ) (#sc-711, RRID:AB_631835) were from Santa Cruz Biotechnology (Dallas, US). Phosphotyrosine Antibody, clone 4G10 (EMD Millipore, Darmstadt, Germany, RRID:AB_2891016). IRAP antibodies used with 3T3-L1 cells was kindly provided by Paul Pilch (Boston University, USA) and GLUT4 for primary adipocytes was kindly provided by Sam Cushman, α-Tubulin (#T9026, RRID:AB_477593, Sigma-Aldrich, St. Louis, USA), Syntaxin-16 (Synaptic System #110 161; RRID:AB_2198368) and Fluorescence-conjugated (Alexa Fluor) secondary antibodies and BODIPY 493/503 (D3922) were purchased from (Molecular Probe, Waltham, United States).

Animals and diet intervention

C57BL6/N mice with global deletion of exon 3 of the *Ehd2* gene (referred to as EHD2 KO or KO in all figures) as described (Matthaeus et al., 2020) were kindly provided by Oliver Daumke (MDC, Germany). Genotyping was carried out to confirm the deletion of the EHD2 gene. EHD2 KO and corresponding control (WT) C57BL6/N mice were bred in parallel to

generate sufficient number of animals for cellular analysis. Animals were kept on a 12 h light cycle with non-restricted food and water supply and were acclimatized one week before starting the intervention. Animals (n=2-5/cage) were fed either chow or HFD (#D12492, 60E % fat, Research Diets, New Brunswick, USA), for 2 weeks. At the time of termination, inguinal adipose tissue were excised, weighed, and used for adipocyte isolation. Data was obtained from male mice at ~12 weeks of age. Terminal serum samples were collected from *vena saphena* for serum cholesterol analysis. All animal procedures were approved by the Malmö/Lund Committee for Animal Experiment Ethics, Lund, Sweden.

Isolation of primary adipocytes

Primary adipocytes were isolated from inguinal adipose tissue depot as described previously (Rodbell, 1964). The cells were suspended in Krebs Ringer Bicarbonate HEPES (KRBH) buffer, pH 7.4, containing 200 nM adenosine, and 3 % (w/v) BSA.

Glucose uptake primary adipocytes

Glucose uptake in primary adipocytes was determined as previously described (Gliemann et al., 1984). Briefly, cells (7.5% (v/v) suspension) were incubated with or without insulin (concentrations shown in figure legends) in KRBH buffer in triplicates for 30 minutes, followed by the addition of D-^{14}C(U)-glucose (2.5 µl/ml, NEC042, Perkin Elmer, Waltham, USA), and an additional 30 min of incubation. The uptake was terminated by spinning 300 µl of each cell suspension in microtubes containing 80 µl dinonylphtalate oil. The cell fraction was collected, dissolved in scintillation fluid (Optima Gold, Perkin Elmer), and subjected to scintillation counting. Glucose uptake in 3T3-L1 adipocytes was performed as outlined (Roccisana et al., 2013).

Western blot analysis

For western blot analysis of basal and insulin stimulated adipocytes, cells were washed with KRBH buffer without BSA before beeing lysed in lysis buffer containing 50 mM Tris/HCl pH 7.5, 1 mM EGTA, 1 mM EDTA, 0.27 M sucrose, 1% NP-40, and complete protease- and phosphatase inhibitor cocktail (Roche, Basel, Switzerland). Cell lysates were centrifuged for 10 min at 13000xg and protein concentrations were determined using the Bradford method (Bradford, 1976). Samples were subjected to polyacrylamide gel electrophoresis and electro-

transfer to nitrocellulose membranes. Membranes were blocked with non-fat dry milk (5% (w/v)) and probed with the indicated antibodies. Detection was performed using horseradish peroxidase-conjugated secondary antibodies and enhanced chemiluminescence reagent. The signal was visualized using a BioRad Image camera (Biorad, Hercules, USA). HSP90, α-tubulin or Na^+/K^+-ATPase were used throughout as loading controls.

TIRF imaging

For TIRF imaging we used a commercial TIRF system based on a Nikon Ti-E eclipse microscope equipped with a 100× Apo TIRF DIC oil immersion objective NA of 1.49 (Nikon Instrments Inc.), an iXon Ultra DU-897 EMCCD camera (Andor Technology Ltd.), and four main lasers, 405 nm (Cube, Coherent Inc), 488 nm (Melles-Griot), 561 nm (Sapphire, Coherent Inc), and 640 nm (Cube, Coherent Inc) with corresponding filter sets. Isolated cells were fixed using 4% PFA and labeled with antibodies in a buffer containing 1% BSA, 1% goat serum, and 0.05% saponin, 1 hour per labeled antibody, and imaged as previously described (Wasserstrom et al., 2018). Puncta detection was performed to identify GLUT4 storage vesicles (GSV) using Blob Finder (ZEISS Arivis software) at size cutoff set at <140 nm stepwise for each chanel. Assuming that GLUT4 and IRAP signals from puncta detected within 40 nm distance arise from the same object, and thus resembles GSV, was calculated as percentage of double-positive puncta of total number of GLUT4 positive punctae below 140 nm.

RNA seq analysis

RNA seq analysis data originates from Hansson et al 2018. Data analysis was performed accordingly.

RT-qPCR

Total RNA was extracted using miRNeasy mini kit (Qiagen #74104). RNA purity and concentration was assessed using a Nanodrop spectrophotometer (Thermo Scientific). RT-qPCR analysis was performed using the Quantifast SYBR Green RT-PCR kit (Qiagen #204156) and Quantitect primer assays for *18S* (QT02448075) and *Insr_1* (QT00287903). Primer sequences are considered proprietary information by Qiagen. mRNA expression levels were measured using a StepOnePlus real-time thermal cycler (Applied Biosystems Waltham,

United States) and displayed as $dCT=CT_{ref} - CT_{goi}$. 18S rRNA was used for normalization (CT_{ref}).

Plasma membrane fractionation

Plasma membrane fractions for determination of insulin-stimulated GLUT4 translocation were prepared using a method described by (Nishiumi and Ashida, 2007). Briefly, isolated adipocytes were incubated with our without insulin (1 nM) for 30 min. Subsequently, cells were washed with KRBH without BSA twice and lysed in a buffer containing 50 mM Tris/HCl pH 8.0, 0.5 mM DTT, 0.1% NP-40 and additional protease and phosphatase inhibitors (complete Ultra, Phospho-Stop, Roche, Basal, Switzerland). Cell lysates were centrifuged at 1000xg, 10 min, 4°C. The fat layer was removed and the pellet was washed in 50 mM Tris/HCl pH 8.0, 0.5 mM DTT, and additional protease and phosphatase inhibitors. The supernatant was discarded, and the pellet was dissolved in 50 mM Tris/HCl pH 8.0, 0.5 mM DTT, 1 % NP-40, and additional protease and phosphatase inhibitors. After one hour on top of ice with occasional shaking the dissolved pellet was centrifuged 16 000xg, 20 min, 4°C, and the supernatant was collected as the plasma membrane (PM) fraction. PM fractions were subjected to subsequent western blot analysis.

For assessment of IRβ, CAV1, cavin1, and SNARE protein levels as well as lipidomic analysis, plasma membrane fractions were obtained in a detergent-free way according to a protocol by (Gustavsson et al., 1996). Briefly, primary adipocytes were lysed in buffer containing 10 mM Tris/HCl, pH 7.4, 1 mM EDTA and protease inhibitors (complete Ultra, Phospho-Stop, Roche, Basal, Switzerland) using a dounce homogenizer (all steps are carried out at 0-4°C). Cell debris and nuclei were removed by centrifugation at 400xg for 10 min. A plasma membrane-containing pellet was obtained by centrifugation at 16 000xg for 20 min and was resuspended in 10 mM Tris/HCl, pH 7.4, 1 mM EDTA and protease inhibitors (complete Ultra, Phospho-Stop, Roche, Basal, Switzerland). Purified plasma membranes were obtained by sucrose density gradient centrifugation. Accordingly, the plasma membrane containing suspension was layered on a 1.12 M sucrose cushion and centrifuged for 60 min at 140 000xg. Plasma membrane fractions were collected and centrifuged at 170 000xg for 20 min, the supernatant was discarded and the pellet was used as a the adipocyte plasma membrane fraction for subsequent analysis.

Cell culture

3T3-L1 fibroblasts, purchased from the American Tissue Culture Collection (RRID:CVCL_0123), were grown, maintained and differentiated into mature adipocytes as outlined previously (Sadler et al., 2015, Roccisana et al., 2013). siRNA-mediated gene knockdown in 3T3-L1 adipocytes was performed as previously described (Duan et al., 2022). EHD2 (ThermoFisher MSS281816) or scrambled siRNA (SCR) (Ambion 4390844) was added to 1.2 ml Opti-MEM to a final concentration of 40 nM with 48 µl TransIT-X2 transfection reagent (Mirus Bio). At 6 days post-differentiation, 3T3-L1 adipocytes grown on a 10 cm dish were washed once with PBS, trypsinized with 2 ml Gibco TrypLE Express enzyme, resuspended in DMEM/FBS medium and centrifuged at 200xg for 5 min. The supernatant was removed, and pelleted cells were resuspended in 13.5 ml DMEM/FBS medium. 900 µl cell suspension and 100 µl EHD2 or SCR siRNA/TransIT-X2/Opti-MEM mixture were reseeded onto each well of a 12 well plate. For Proximity Ligation Assays, these wells contained 13 mm glass coverslips. Cells were used in experiments 4 days following siRNA knockdown. Cells were serum starved 2 hours prior to all experiments.

Immunoprecipiation and proteomics

Syntaxin 16 was immunoprecipitated from lysates of day 10 post-differentiation 3T3-L1 adipocytes prepared as described (Bremner et al 2022). 2µg of anti-syntaxin-16 (Synaptic System #110 161; RRID:AB_2198368) was used in an immunoprecipitation from 1mg of adipocyte lysate and the IP'd material separated on SDS-PAGE. All subsequent steps were performed at the FingerPrints Facility, University of Dundee. Samples were washed then reduced/alkylated with DTT/IAA, respectively, then digested overnight (16h) with trypsin (Modified Sequencing Grade, Roche, UK). Peptides were extracted and dried in a SpeedVac, resuspended in 1% formic acid, centrifuged and analysed using an Ultimate 3000 RSLCnano system (Thermo Scientific). Samples were injected and washed on C18 trap with 0.1% formic acid and after 3 minutes wash gradient formed with 0.1% formic acid and 80% acetonitrile on 0.08% formic acid. Peptides were initially trapped on an Acclaim PepMap 100 (C18, 100 µM x 2 cm, Thermo Scientific) and then separated on an Easy-Spray PepMap RSLC C18 column (75 µM x 50 cm, Thermo Scientific). Samples were transferred to LTQ OrbiTrap Velos Pro mass spectrometer via an Easy-Spray source with temperature set to 50 °C and a source

voltage of 2.05 kV. OrbiTrap Velos Pro RAW files were analysed with Proteome Discoverer (Version 1.4) using Mascot (Version 2.4) as search engine. Database used: IPImouse.

Proximity Ligation Assay

Following siRNA knockdown as previously described, 3T3-L1 adipocytes were reseeded onto 13 mm coverslips in 12-well plates. Following stimulation with 100 nM insulin for 5 or 20 min as indicated, cells were washed three times with PBS and fixed for 20 min with 1 ml warm 4% w/v paraformaldehyde. Cells were then washed three times with PBS and incubated with 1 ml quenching buffer (50mM NH_4Cl in PBS) for 10 min followed by a further three washes with PBS. Cells were incubated with 1 ml permeabilization buffer (0.1% v/v Triton X-100 in PBS) for 5 min. Proximity Ligation Assay (PLA) on fixed and permeabilized 3T3-L1 adipocytes was carried out using the NaveniFlex MR kit (Navinci NF.MR.100) according to the manufacturer's instructions. Briefly, cells were blocked to prevent non-specific binding of antibodies before being incubated with a pair of primary antibodies from mouse and rabbit host species respectively; Sx4 (RRID:AB_887853)/Munc18c (#H00006814-B01P, RRID:AB_2302682, Novus, Centennial, US); CAV1 (#ab2910, RRID:AB_303405)/IRβ (#ab69508, RRID:AB_1209215, Abcam); VAMP2 (#104211, RRID:AB_887811, Synaptic systems)/Munc18c(ab224625);SNAP23 (RRID:AB_10805651)/VAMP2 (RRID:AB_887811); SNAP23 (RRID:AB_10805651)/Munc18c (RRID:AB_2302682). Cells were then incubated with a pair of anti-mouse and anti-rabbit navenibodies before undergoing a series of enzymatic reactions prior to the application of the detection fluorophore. Following the NaveniFlex PLA protocol, cells were incubated with 1 µg/ml 4',6-diamidino-2-phenylindol (DAPI) to stain DNA. All incubations took place in a humidity chamber at 37°C and cells were washed with TBST (20 mM Tris/HCl, 150 mM NaCl, 0.05 % (v/v) Tween) between each step. All reaction volumes were 40 µl per 13 mm coverslip. Signals were visualized using a Leica TCS SP8 system with a 63×oil immersion objective. For quantification, signals in 50 to 70 imaged cells per experimental condition were counted in ImageJ, using the protocol and parameters previously described (Lopez-Cano et al., 2019). Statistical analyses were done by two-way ANOVA testing. Figures and plots are representative of results from 3 independent experiments.

Lipidomics

Detergent free plasma membrane fractions were prepared as described above. Lipids were extracted and samples prepared as previously elucidated in detail (Herzog et al., 2020), with the only exception being the fat cake, which was evaporated and directly dissolved in isopropanol/water (9/1, v/v). Lipidomic analyses were performed on an Agilent 1290 Infinity UHPLC system coupled to an Agilent 6495 QqQ-MS (Agilent Technologies, Santa Clara, CA) operated in dynamic multiple-reaction-monitoring (MRM) mode. Separation of lipids was performed as previously described (Herzog et al., 2020). The mass spectrometer was operated in positive and negative electrospray ionization mode (ESI^+ and ESI^-, respectively) with a fragmentor voltage of 380 V, a cell acceleration voltage of 5 V, a gas temperature of 200°C, a gas flow rate of 14 l/min, a nebulizer pressure of 20 psi, a sheath gas temperature of 250°C, and a sheath gas flow-rate of 11 l/min. The capillary voltage was 3000 V for ESI^+ and 2500 V for ESI^-, the high/low pressure iFunnel RF was 200/100 V and 90/60 V for ESI^+ and ESI^-, respectively, and the nozzle voltage 1500 V for both modes. MRM transitions were based on (Takeda et al., 2018) and are given in Supplemental Table S1 (ESI^+) and Supplemental Table S2 (ESI^-). Data were processed using MassHunter Qualitative Analysis and Quantitative Analysis (Agilent Technologies, Santa Clara, CA). Cholesterol levels were measured in plasma membrane, fat cake and serum samples collected from WT and EHD2 KO mice (Fryklund et al., 2021) by gas chromatography mass spectrometry, as previously described in detail (Danielsson et al., 2010).

Statistical analyses

Statistical analysis was carried out as indicated in each figure legend using GraphPad Prism 9 (GraphPad Software Inc.) software. Proximity Ligation Assay data were analyzed using two-way ANOVA testing performed in R using RStudio. Significance was determined according to *=$p \leq 0.05$, **=$p \leq 0.01$, ***=$p \leq 0.001$ and ****=$p \leq 0.0001$. All data are displayed as mean±SD. Lipidomic data were analysed in R 3.6.1 using ANOVA (aov), principal component analysis (PCA; prcomp), the Student´s t-test (t.test) and the chi-square test (chisq.test) from the stats package. Orthogonal projections to latent structures discriminant analysis (OPLS-DA) was conducted using opls (ropls package). p-values are reported as q-values after adjustment for multiple testing using the Benjamini-Horchberg method (p.adjust, stats). Data were illustrated using ggplot (ggplot2).

Results

EHD2 deficiency impairs GLUT4 translocation and glucose uptake in adipocytes

Previously, we identified EHD2 as one of the highest upregulated genes in white adipose tissue in response to short-term high fat diet (HFD)-feeding (Figure 1A) (Data retrieved from RNA sequencing performed in a previous study (Hansson et al., 2018)). This finding suggests that EHD2 plays a key role during the development of overweight and obesity. Accordingly, we chose to monitor the impact of EHD2 deficiency on cellular glucose transport, both in the chow-fed state as well as after 2 weeks of HFD to resolve possible differences related to the degree of adipose tissue expansion. Therefore, we analysed glucose uptake in primary inguinal adipocytes isolated from EHD2 KO mice and corresponding control (WT) mice. While both non- and insulin-stimulated glucose uptake were similar in EHD2 KO and WT adipocytes in the chow-fed state (Figure 1B), we found a significant reduction in both basal and insulin-stimulated glucose uptake (~30% basal, ~45% insulin) in EHD2 KO adipocytes compared with WT adipocytes isolated from HFD-fed mice (Figure 1C). This finding was confirmed using a non-metabolizable 2-Deoxy-D-glucose tracer, the data of which indicates that glucose uptake, rather than glucose metabolism, is reduced in EHD2 deficient adipocytes (Figure 1D). Taken together, lack of EHD2 affected glucose uptake in the obese but not chow-fed state. As EHD2 expression is highly upregulated during HFD and differences in glucose uptake are only observable in adipocytes from HFD-fed mice, we focused on examining the mechansims of EHD2 in adipocytes in cells isolated after short-term HFD-feeding.

Total cellular GLUT4 levels were similar in whole cell lysates of WT and EHD2 KO adipocytes in the HFD-fed animals (Figure 1E). However, and consistent with glucose transport assays, the ability of insulin to increase PM GLUT4 levels was markedly lower in EHD2 KO adipocytes (Figure 1F). This data argues for an impairment in insulin-stimulated GLUT4 translocation in EHD2 KO adipocytes despite normal levels of total cellular GLUT4 in these animals. Intriguingly, we observed similar fold increase of IRAP in the PM of both WT and EHD2 KO adipocytes after insulin stimulation (Supplementary Figure S1A). Further, TIRF microscopy demonstrated that EHD2 KO adipocytes display lowered GSV number in the basal state (Figure 1H-I). Hence, the lower basal rate of glucose transport in EHD2 KO cells could be related to changes in GSV formation as well as expression of other GLUT isoforms such as GLUT1 which is known to contribute to basal glucose uptake. This is supported by the notion that we observed similar levels of GLUT4 in the basal state in WT and EHD2 KO cells using PM sedimentation assay (Figure 1G) and TIRF imaging (Figure

1I). Furthermore, we observed that basal IRAP levels in PM proximity are similar in WT and EHD2 KO accessed by both PM sedimentation assay (Supplement Figure 1A (right)) and TIRF imaging (Figure 1I).

Reduced caveolae protein expression, insulin receptor stability and downstream insulin signalling in EHD2 KO cells

Next, we examined whether impaired insulin signal transduction could explain the lowered glucose uptake observed in EHD2 deficient cells. Western blot analysis showed lowered insulin-stimulated phosphorylation of IRS-1 (Y612), Akt (S473) and AS160 (T642) at maximal insulin concentrations in EHD2 KO adipocytes compared to WT (Figure 2A-C). Further, we found a reduction in sub-maximal insulin-stimulated phosphorylation of IRS-1 (Y612) (Figure 2A) and slighty reduced submaximal phosphorylation of Akt (S473, p~0.068) (Figure 2B).

Protein expression of IRS-1, Akt and AS160 in the basal state were similar comparing WT and EHD2 KO (Figure 2D-E and quantifications displayed as phospho/total protein levels for each target are shown in Supplementary Figure S1B). For comparison insulin signaling in WT and EHD2 deficient adipocytes in the CHOW-fed state is presented in Supplementary Figure S1C.

As the insulin receptor (IR) is located and stabilized at caveolae and is relying on caveolar integrity to function, we next assessed expression of both IR and the core-caveolaer proteins CAV1 and cavin1. We found a significant decrease (~50%) in both total and plasma membrane-associated IRβ levels (Figure 3A-B, see Supplementary Figure S1D for chow IRβ levels) in adipocytes from EHD2 KO mice compared with WT, whereas RT-qPCR analysis showed similar insulin receptor (*Insr*) mRNA expression (Figure 3C). Further, both CAV1 and cavin1 were significantly downregulated in both whole-cell lysates (~60 and ~40%, respectively, 3D) and plasma membrane fraction (~65%, 3E) in EHD2 KO adipocytes compared to WT.

To adress whether EHD2 knockdown affects IRβ and CAV1 interaction we used proximity ligation assays (PLA) to probe the interaction between these proteins *in situ* in siRNA-mediated EHD2 gene silenced (EHD2 KD) 3T3-L1 adipocytes. Consistent with our observations in primary adipocytes, EHD2 KD in 3T3-L1 cells reduced IRβ and CAV1 expression (~50% and 20%, respectively) (Figure 3F). PLA revealed a previously undescribed insulin-dependent reduction in the interaction between CAV1 and IRβ upon

insulin stimulation in control cells (60% reduction 20 min after exposure to insulin), confirming and extending previous work identifying an important role for caveolae in insulin receptor signalling. Interestingly, we observed that the CAV1-IRβ interaction was significantly lower for EHD2 KD cells under all conditions tested, and insulin was without effect (Figure 3G). It should be noted that although the total cellular levels of these proteins are reduced in EHD2 KO adipocytes compared to WT which may account for the reduced interactions in the absence of insulin, here we also compare interactions in response to insulin within each group which are independent of levels.

Together, these findings suggest that the lack of EHD2 alters caveolae integrity, which in turn negatively influences IRβ stability at the plasma membrane and downstream insulin signalling, ultimaltey reducing insulin-stimulated glucose uptake.

Insulin-stimulated SNARE protein complex formation is impaired in EHD2 depleted 3T3-L1 adipocytes

To verify our findings in another adipocyte model and to examine if our findings are related to EHD2 deficiency in adipocytes specifically (and not other factors related to whole-body EHD2 KO influencing adipocyte function), we made use of siRNA-mediated EHD2 gene silencing (EHD2 KD) in 3T3-L1 adipocytes.

Using a total-phosphotyrosine antibody, we found overall lowered insulin-induced tyrosine phosphorylation (Figure 4A) and impaired insulin-stimulated glucose uptake (Figure 4B) but similar GLUT4 levels (Figure 4C) in EHD2 KD cells consistent with findings described above in primary adipocytes. Because SNARE proteins underpin the fusion of GSV with the cell surface, we examined the expression of SNARE proteins in EHD2 KD cells. Both the t-SNARE SNAP23 and the SNARE regulatory protein Munc18c were significantly lower (~40%) in EHD2 KD compared to control (Figure 4C), while total cellular expression of VAMP2, Syntaxin 4 and 16, SNARE proteins implicated in GLUT4 trafficking (Bryant et al., 2002), remained unaltered (Figure 4C).

To adress whether EHD2 KD affects the formation of the SNARE complexes required for GSV fusion, we used PLA to probe interactions between SNARE proteins *in situ* in control and EHD2 KD cells that were insulin-stimulated for 5 or 20 min or left untreated (Basal) (Figure 5). We observed significant transient increases in insulin-stimulated interactions between SNAP23/VAMP2 and SNAP23/Munc18c in control cells (time point 5 min)

consistent with previous studies (Kioumourtzoglou et al., 2014). In marked contrast these interactions were not affected by insulin in EHD2 KD cells (Figure 5). In line with previous reports (Kioumourtzoglou et al., 2014), we found no effect of insulin on interactions between VAMP2/Munc18c or Syntaxin4/Munc18c in either WT or EHD2 KD cells (Figure 5). These data underscore the importance of EHD2 to facilitate the formation of key SNARE complexes involved in insulin-stimulated GSV fusion events at the plasma membrane.

EHD2 deficiency is associated with decreased Syntaxin 4 level and altered lipid composition in plasma membrane

In an attempt to understand how EHD2 deficiency could impact SNARE complex formation, we turned back to primary adipocytes. Adipocytes from EHD2 KO did not exhibit altered total levels of Sx4 (or SNAP23 and Munc18c) (Figure 6A). However, Sx4 levels were strikingly reduced (~40%) in the plasma membrane enriched fraction of EHD2 KO adipocytes (Figure 6B).

As both the structure of individual SNARE proteins (Fezoua-Boubegtiten et al., 2019, Lakomek et al., 2019, Wang et al., 2020, Saito et al., 2012), their localization to specific plasma membrane domains (Chamberlain et al., 2001, Salaun et al., 2005, Lang et al., 2001) and the process of SNARE protein complex formation as well as GLUT functionality (Hresko et al., 2016) is influenced by lipid environment, we next performed lipidomic analysis of isolated primary adipocytes to resolve if differences in plasma membrane composition could contribute to the lowered insulin-induced effects in EHD2 KO adipocytes. Consistent with this idea, we observed lower levels of cholesterol in the plasma membrane fraction of EHD2 KO adipocytes, whereas no differences were observed in the isolated fat cake fraction (Figure 6C). This alteration does not reflect a global lipid remodulation, as serum levels of cholesterol were higher in the EHD2 KO mice (Figure 6C). One possible explanation of this observation stems from work implicating Syntaxin6 (Sx6) in the delivery of microdomain-associated lipids and proteins to the cell surface. Sx6 is the $Q_{b,c}$ SNARE syntaxin that forms a functional tSNARE with the Q_a SNARE Sx16 (Wang et al., 2017) and plays a key role in sorting GLUT4 through the endosomal system. Disruption of Sx6 impairs delivery of caveolar proteins to the cell surface (Choudhury et al., 2006), indicating that cholesterol, caveolae and Sx6/16 are functionally linked. Mass Spec analysis of proteins co-immunoprecipiated with Sx16 identified EHD2 as an associated protein (Table 1). Analysis of this data revealed that it was the major protein in the immunoprecipitated sample, and peptides corresponding to 77%

of the EHD2 protein were identified. Importantly, EHD2 was more abundant in these immunoprecipitates than mVps45, the Sec1/Munc18 binding partner of Sx16 (Table 1).

With respect to the lipid profile, PCA revealed a systematic difference in the membrane fraction and serum between the EHD2 KO mice and WT, but not so for the fat cake (Supplemental Figure S2). These changes were investigated in more detail using OPLS-DA, revealing a systematic difference in plasma membrane lipidome between WT and EHD2 KO mice (Figure 6D-E). Notably, an enrichment of phosphatidylethanolamine (PE), PE ether lipids (PE_ep), phosphatidylcholine (PC), and sphingomyelin (SM) were found among significantly altered lipids, all of which showing lower levels in adipocyte plasma membranes from EHD2 KO mice. No systematic difference was observed in the fat cake and in the serum lipidomes. Possibly, these differences in membrane lipid composition are related to the changes in insulin-mediated SNARE complex formation, insulin receptor stability and GLUT4 integrity and vesicle fusion.

Discussion

We previously confirmed a central role of EHD2 to sustain lipid metabolism (Fryklund et al., 2021). In the latter study, we found that insulin-induced inhibition of adipocyte lipolysis was diminished in EHD2 KO mice (Fryklund et al., 2021), and therefore we set out to explore if other insulin-regulated cellular processes were affected in EHD2 deficient cells. Further, we could also elucidate in the respective study that 2w of HFD serves as a time-point at which we can observe similar adipocyte size in EHD2 KO and WT adipocytes, excluding that the observed differences are due to changes in adipocyte size (Fryklund et al., 2021).

In this study, we demonstrate that both basal and insulin-stimulated glucose uptake are impaired in EHD2 KO adipocytes after short-term HFD-feeding. These findings are in line with previous findings from Park *et. al.*, reporting that inhibition of EHD2 (using an EHD2-specific antibody) is associated with impaired insulin-stimulated GLUT4 translocation in primary rat adipocytes (Park et al., 2004). Consistent with this, we observed reduced insulin-stimulated glucose uptake and GLUT4 translocation in EHD2 KO adipocytes compared to WT controls (Figure 1). The fact that we see comparable differences in both glucose tracer uptake assays using either a metabolized or a non-metabolized glucose tracer) suggests that the differences in glucose uptake originate from impaired glucose transport rather than metabolism (Figure 1). The differences in basal glucose uptake could be linked to the reduced number of GSVs in EHD2 KO adipocytes, which could consequently lead to altered GLUT4

cycling. Our results demonstrate similar GLUT4 expression and similar basal GLUT4 in PM in both genotypes (EHD2 KO and WT; Figure 1E, G and I) and thus suggest that mechanisms other than those related to GLUT4 levels contribute to diminshed glucose uptake. Rather, we observed a decreased magnitude of GLUT4 translocation in EHD2 KD adipocytes, prompting us to consider the mechanisms which may underlie this.

We observed significantly impaired phosphorylation of key insulin signalling mediators IRS-1 (Y612), Akt (S473), and AS160 (Thr642) (Figure 2), which may contribute to the observered decrease in insulin-stimulated glucose uptake in EHD2 KO adipocytes. These findings were replicated using siRNA-mediated EHD2 KD in 3T3-L1 cells, which also resulted in reduced insulin signal transduction and lowered insulin-stimulated glucose uptake (Figure 4). However, proximal insulin signalling holds a high spareness, meaning that reduced phosphorylation of IRS-1 and Akt can still induce maximal biological response to insulin. Therefore maintained glucose uptake could be observed despite impaired proximal insulin signalling (Frank et al., 1981, James et al., 2021).

In search for the cause behind impaired insulin signalling, we found significantly reduced protein levels of IRβ, CAV1 and cavin1 (total and plasma membrane-localized) in EHD2 KO adipocytes, without reduced insulin receptor mRNA levels (Figures 3). These observations suggest that EHD2 deficiency negatively affects IRβ stability. In support of this, Cohen *et. al.* showed that CAV1 deficiency evokes proteosomal degradation of the insulin receptor (Cohen et al., 2003), and CAV1 knockdown is associated with reduced stability and diminished expression of IRβ and GLUT4 in 3T3-L1 adipocytes (Gonzalez-Munoz et al., 2009). Further, data from Nystrom *et al.* elucidated that IRβ contains a CAV1 specific-binding motif; upon CAV1 knockout this binding was disrupted, resulting in markedly decreased cell surface insulin receptor expression and a defect in IRβ autophosphorylation (Nystrom et al., 1999). Consistent with this, Yamamoto *et al.* demonstrated that caveolin controls IRβ kinase activity in 293T cells (Yamamoto et al., 1998). Using PLA we revealed an interaction between CAV1 and IRβ in control cells, which significantly decreased in response to insulin (Figure 3). This is in line with the notion that caveolae-associated insulin receptors are a key focal point of insulin signalling, and that IRβ levels in caveolae fall in response to insulin treatment, possibly reflecting the subsequent ligand-induced internalization of the receptor which is known to be necessary to propagate insulin signalling (Hall et al., 2020). Interestingly, CAV1-IRβ interaction was significantly reduced in EHD2 KD cells in the basal state and was not sensitive to insulin, in contrast to control cells. While the insulin receptor was shown to both localize and function in caveolae (Gustavsson et al., 1999), Foti *et al.* demonstrated that the

insulin receptor is specifically enriched at the neck of caveolae, suggesting that EHD2 and the insulin receptor are found in close proximity in caveolae (Foti et al., 2007). Our data indicate that EHD2 is necessary to sustain insulin receptor downstream signalling, probably mediated through a caveolae-dependent insulin receptor stabilization, which preserves insulin receptor autophosphorylation.

Mattheus *et al.* could previously demonstrate that the amount of membrane-detached caveolae is increased in white adipose tissue from EHD2 KO mice (Matthaeus et al., 2020). Accordingly, we observed irregular caveolae shape and size in EHD2 deficient primary adipocytes in our previous study (Fryklund et al., 2021). The significantly decreased plasma membrane content of the caveolar core proteins CAV1 and cavin1, presented in the current study (Figure 3) is consistent with the hypothesis that caveolae integrity is potentially altered in EHD2 deficient cells. In support of this, we observed lowered cholesterol and decreased levels of sphingomyelin, phosphatidylethanolamine, phosphatidylcholine in the plasma membrane from EHD2 KO adipocytes, indicating that a large share of caveolae-characterizing lipids are less abundant in the plasma membrane of these adipocytes. These observations are supported by studies which have linked Sx6/Sx16 function with the delivery of cholesterol and cavaeolae components to the cell surface (Choudhury et al., 2006, Wang et al., 2017). Here we show that EHD2 interacts directly with Sx16 (Table 1), and thus identify a potential link between EHD2 function and both caveolar integrity and insulin signalling. This is supported by studies using Methyl-β-cyclodextrin-induced caveolae depletion which revealed a causal link between caveolae intergrity, insulin signal transduction and glucose uptake (Parpal et al., 2001, Karlsson et al., 2004). Herein, we demonstrate that insulin receptor stability and downstream signalling events are impaired concurrently with altered plasma membrane lipid and protein profile in EHD2 deficient adipocytes. This is firmly in line with previous reports showing a strong relation between IRβ signalling and plasma membrane lipid environment, including caveolae lipid microenviroment, as a controlling agent of IRβ function and downstream signalling (Yamamoto et al., 1998, Suresh et al., 2021, Perona, 2017, Foti et al., 2007). We further extend these observations to suggest a novel interaction between EHD2 and Sx16 may underpin these observations, but further studies are required to define these observations mechanistically.

It is well established that not only the insulin receptor but also the localisation, assembly and function of SNARE proteins as well as GLUT integrity is influenced by the membrane lipid composition. Proteomic studies have shown an enrichment of SNAP isoforms and the vesicle SNARE protein VAMP2 in isolated caveolae fractions (Schnitzer et al., 1995, Matthaeus and

Taraska, 2020) and cholesterol levels are known to influence the function of key SNARE proteins involved in insulin-stimulated GLUT4 translocation to the cell surface (Chamberlain and Gould, 2002). Additionally, it has been postulated that membrane lipid-remodulation is initiated by protein-dependent formation of membrane heterogeneities, which then are stabilized by recruitment of lipids (Harayama and Riezman, 2018). Hence, an altered expression of EHD2 may promote changes in lipid rafts or other plasma membrane cholesterol-containing domains, perhaps by Sx16-dependent mechanisms. Notably, among the lipids showing reduced plasma membrane levels in EHD2 KO, we found the bilayer-disrupting lipid classes PE and the related ether lipids (PE_ep) (Figure 6), which are crucial mediators of fusion and fission events (Harayama and Riezman, 2018). Moreover, levels of both cholesterol and SM lipids were reduced (Figure 6), emphasising their co-existence in in membrane nanodomains (Sezgin et al., 2017). Importantly, Hresko et al. demonstrated that PE, PC and Cholesterol (lipids we also identified as crucially reduced in EHD2 KO plasmamembranes) are among the membrane lipids that exert the most critical effects on GLUT4 transport capacity and GLUT4 stabilization (Hresko et al., 2016), possibly explaining the herein observed differences in glucose uptake.

The differences in plasma membrane cholesterol and lipid composition detected in EHD2 depleted cells may also contribute to the impaired SNARE protein assembly revealed from our PLA analysis (Figure 5). Our previous studies identified an insulin-dependent increase in SNARE complex formation, revealed by increases in PLA signal between SNAP23 and VAMP2, and SNAP23 and Munc18c five minutes after exposure to insulin (Kioumourtzoglou et al., 2014); a result recapitulated here (Figure 5). In marked contrast, EHD2 KD cells did not exhibit these insulin-dependent changes, despite broadly similar PLA signals in the absence of insulin. One interpretation of these data is that EHD2 KD results in impairment of early events (5 minutes after exposure to insulin) in GLUT4 trafficking. We and others have reported a cholesterol-dependent clustering of the SNARE proteins involved in GLUT4 vesicle fusion with the plasma membrane (Lang et al., 2001, Chamberlain and Gould, 2002), hence the impairment in SNARE function in EHD2 KD cells might explain the observed reduction in insulin-stimulated glucose transport (Figure 4). The fact that we found reduced expression of syntaxin 4 in the plasma membrane, but not total cell lysates, in EHD2 KO inguinal adipocytes (Figure 6) further emphasizes that SNARE distribution is impaired in EHD2 KO adipocytes, which indeed could contribute to impaired GLUT4 exocytosis and hence lowered glucose uptake.

In conclusion, we present data that emphasize the importance of caveolae integrity for insulin signalling and glucose uptake. Further, our data suggests that EHD2 deficiency negatively influences IRβ stability, caveolin-1-IRβ interaction, insulin signalling and downstream events including SNARE protein complex formation and GSV fusion. We hypothesize these alterations are caused by impaired caveolae integrity and altered membrane lipid composition, which in turn influences IR stability and membrane trafficking events.

Acknowledgements

We would like to thank Maria Lindahl and Tina Ovlund for excellent technical support and we would also like to thank Lund University Bioimaging Center (LBIC) for assistance with imaging sample preparation. Further, we would like to thank Dougie Lamont, FingerPrints for help with the MS analysis and interpretation. This work was financially supported by the Swedish Research Council (2019-00978) and Strategic Research Area Exodiab (2009-1039)), the Swedish Foundation for Strategic Research (IRC15-0067), Novo Nordisk (NNF20OC0063659), Swedish Diabetes Foundation, The Crafoord Foundation, and Albert Påhlsson Foundation. Holly Taylor was supported by a Diabetes UK PhD studentship (18/0005905 to GWG and NJB) and Diabetes UK grants (18/0005847 and 15/0005246 to GWG and NJB).

Author contribution

CF, MN, BM, FK, OR, HA, PS, HT, SKB, NJB, GWG and KS conceived and designed the experiments. CF, MN, BM, FK, OR, HA, PS, HT, LS, NJB, GWG and KS collected, analysed and interpreted data. MN, and KS drafted the article and CF, BM, FK, OR, HA, PS, HT, NJB, GWG and KS revised it critically for important intellectual content. All authors made comments on the manuscript and approved the final version submitted for publication. All persons designated as authors qualify for authorship, and all those who qualify for authorship are listed.

Competing interests

The authors declare that the research was conducted in the absence of any commercial or financial relationships that could be construed as a potential conflict of interest.

References

Acosta, J. R., Douagi, I., Andersson, D. P., Backdahl, J., Ryden, M., Arner, P. & Laurencikiene, J. (2016). Increased fat cell size: a major phenotype of subcutaneous white adipose tissue in non-obese individuals with type 2 diabetes. *Diabetologia,* 59**,** 560-70. 10.1007/s00125-015-3810-6

Bradford, M. M. (1976). A rapid and sensitive method for the quantitation of microgram quantities of protein utilizing the principle of protein-dye binding. *Anal Biochem,* 72**,** 248-54. 10.1006/abio.1976.9999

Bryant, N. J., Govers, R. & James, D. E. (2002). Regulated transport of the glucose transporter GLUT4. *Nat Rev Mol Cell Biol,* 3**,** 267-77. 10.1038/nrm782

Chamberlain, L. H., Burgoyne, R. D. & Gould, G. W. (2001). SNARE proteins are highly enriched in lipid rafts in PC12 cells: implications for the spatial control of exocytosis. *Proc Natl Acad Sci U S A,* 98**,** 5619-24. 10.1073/pnas.091502398

Chamberlain, L. H. & Gould, G. W. (2002). The vesicle- and target-SNARE proteins that mediate Glut4 vesicle fusion are localized in detergent-insoluble lipid rafts present on distinct intracellular membranes. *J Biol Chem,* 277**,** 49750-4. 10.1074/jbc.M206936200

Chen, Y., Huang, L., Qi, X. & Chen, C. (2019). Insulin Receptor Trafficking: Consequences for Insulin Sensitivity and Diabetes. *Int J Mol Sci,* 20 10.3390/ijms20205007

Choudhury, A., Marks, D. L., Proctor, K. M., Gould, G. W. & Pagano, R. E. (2006). Regulation of caveolar endocytosis by syntaxin 6-dependent delivery of membrane components to the cell surface. *Nat Cell Biol,* 8**,** 317-28. 10.1038/ncb1380

Cohen, A. W., Razani, B., Wang, X. B., Combs, T. P., Williams, T. M., Scherer, P. E. & Lisanti, M. P. (2003). Caveolin-1-deficient mice show insulin resistance and defective insulin receptor protein expression in adipose tissue. *Am J Physiol Cell Physiol,* 285**,** C222-35. 10.1152/ajpcell.00006.2003

Danielsson, A. P., Moritz, T., Mulder, H. & Spegel, P. (2010). Development and optimization of a metabolomic method for analysis of adherent cell cultures. *Anal Biochem,* 404**,** 30-9. 10.1016/j.ab.2010.04.013

Daumke, O., Lundmark, R., Vallis, Y., Martens, S., Butler, P. J. & McMahon, H. T. (2007). Architectural and mechanistic insights into an EHD ATPase involved in membrane remodelling. *Nature,* 449**,** 923-7. 10.1038/nature06173

Duan, X., Norris, D. M., Humphrey, S. J., Yang, P., Cooke, K. C., Bultitude, W. P., Parker, B. L., Conway, O. J., Burchfield, J. G., Krycer, J. R., Brodsky, F. M., James, D. E. & Fazakerley, D. J. (2022). Trafficking regulator of GLUT4-1 (TRARG1) is a GSK3 substrate. *Biochem J,* 479**,** 1237-1256. 10.1042/BCJ20220153

Fagerholm, S., Ortegren, U., Karlsson, M., Ruishalme, I. & Stralfors, P. (2009). Rapid insulin-dependent endocytosis of the insulin receptor by caveolae in primary adipocytes. *PLoS One,* 4**,** e5985. 10.1371/journal.pone.0005985

Fezoua-Boubegtiten, Z., Hastoy, B., Scotti, P., Milochau, A., Bathany, K., Desbat, B., Castano, S., Oda, R. & Lang, J. (2019). The transmembrane domain of the SNARE protein VAMP2 is highly sensitive to its lipid environment. *Biochim Biophys Acta Biomembr,* 1861**,** 670-676. 10.1016/j.bbamem.2018.12.011

Foti, M., Porcheron, G., Fournier, M., Maeder, C. & Carpentier, J. L. (2007). The neck of caveolae is a distinct plasma membrane subdomain that concentrates insulin receptors in 3T3-L1 adipocytes. *Proc Natl Acad Sci U S A,* 104**,** 1242-7. 10.1073/pnas.0610523104

Frank, H. J., Davidson, M. B. & Serbin, P. A. (1981). Insulin binding and action in isolated rat hepatocytes: evidence for spare receptors. *Metabolism,* 30**,** 1159-64. 10.1016/0026-0495(81)90035-4

Fryklund, C., Moren, B., Shah, S., Grossi, M., Degerman, E., Matthaeus, C. & Stenkula, K. G. (2021). EH Domain-Containing 2 Deficiency Restricts Adipose Tissue Expansion and Impairs Lipolysis in Primary Inguinal Adipocytes. *Front Physiol,* 12**,** 740666. 10.3389/fphys.2021.740666

Ginsberg, B. H., Brown, T. J., Simon, I. & Spector, A. A. (1981). Effect of the membrane lipid environment on the properties of insulin receptors. *Diabetes,* 30**,** 773-80. 10.2337/diab.30.9.773

Gliemann, J., Rees, W. D. & Foley, J. A. (1984). The fate of labelled glucose molecules in the rat adipocyte. Dependence on glucose concentration. *Biochim Biophys Acta,* 804**,** 68-76. 10.1016/0167-4889(84)90100-9

Gonzalez-Munoz, E., Lopez-Iglesias, C., Calvo, M., Palacin, M., Zorzano, A. & Camps, M. (2009). Caveolin-1 loss of function accelerates glucose transporter 4 and insulin receptor degradation in 3T3-L1 adipocytes. *Endocrinology,* 150**,** 3493-502. 10.1210/en.2008-1520

Gustavsson, J., Parpal, S., Karlsson, M., Ramsing, C., Thorn, H., Borg, M., Lindroth, M., Peterson, K. H., Magnusson, K. E. & Stralfors, P. (1999). Localization of the insulin receptor in caveolae of adipocyte plasma membrane. *FASEB J,* 13**,** 1961-71.

Gustavsson, J., Parpal, S. & Stralfors, P. (1996). Insulin-stimulated glucose uptake involves the transition of glucose transporters to a caveolae-rich fraction within the plasma membrane: implications for type II diabetes. *Mol Med,* 2**,** 367-72.

Hall, C., Yu, H. & Choi, E. (2020). Insulin receptor endocytosis in the pathophysiology of insulin resistance. *Exp Mol Med,* 52**,** 911-920. 10.1038/s12276-020-0456-3

Hansson, B., Wasserstrom, S., Moren, B., Periwal, V., Vikman, P., Cushman, S. W., Goransson, O., Storm, P. & Stenkula, K. G. (2018). Intact glucose uptake despite deteriorating signaling in adipocytes with high-fat feeding. *J Mol Endocrinol,* 60**,** 199-211. 10.1530/JME-17-0195

Harayama, T. & Riezman, H. (2018). Understanding the diversity of membrane lipid composition. *Nat Rev Mol Cell Biol,* 19**,** 281-296. 10.1038/nrm.2017.138

Herzog, K., Berggren, J., Al Majdoub, M., Balderas Arroyo, C., Lindqvist, A., Hedenbro, J., Groop, L., Wierup, N. & Spegel, P. (2020). Metabolic Effects of Gastric Bypass Surgery: Is It All About Calories? *Diabetes,* 69**,** 2027-2035. 10.2337/db20-0131

Hresko, R. C., Kraft, T. E., Quigley, A., Carpenter, E. P. & Hruz, P. W. (2016). Mammalian Glucose Transporter Activity Is Dependent upon Anionic and Conical Phospholipids. *J Biol Chem,* 291**,** 17271-82. 10.1074/jbc.M116.730168

James, D. E., Stockli, J. & Birnbaum, M. J. (2021). The aetiology and molecular landscape of insulin resistance. *Nat Rev Mol Cell Biol,* 22**,** 751-771. 10.1038/s41580-021-00390-6

Karlsson, M., Thorn, H., Danielsson, A., Stenkula, K. G., Ost, A., Gustavsson, J., Nystrom, F. H. & Stralfors, P. (2004). Colocalization of insulin receptor and insulin receptor substrate-1 to caveolae in primary human adipocytes. Cholesterol depletion blocks insulin signalling for metabolic and mitogenic control. *Eur J Biochem,* 271**,** 2471-9. 10.1111/j.1432-1033.2004.04177.x

Kioumourtzoglou, D., Gould, G. W. & Bryant, N. J. (2014). Insulin stimulates syntaxin4 SNARE complex assembly via a novel regulatory mechanism. *Mol Cell Biol,* 34**,** 1271-9. 10.1128/MCB.01203-13

Lakomek, N. A., Yavuz, H., Jahn, R. & Perez-Lara, A. (2019). Structural dynamics and transient lipid binding of synaptobrevin-2 tune SNARE assembly and membrane fusion. *Proc Natl Acad Sci U S A,* 116**,** 8699-8708. 10.1073/pnas.1813194116

Lang, T., Bruns, D., Wenzel, D., Riedel, D., Holroyd, P., Thiele, C. & Jahn, R. (2001). SNAREs are concentrated in cholesterol-dependent clusters that define docking and fusion sites for exocytosis. *EMBO J,* 20**,** 2202-13. 10.1093/emboj/20.9.2202

Lopez-Cano, M., Fernandez-Duenas, V. & Ciruela, F. (2019). Proximity Ligation Assay Image Analysis Protocol: Addressing Receptor-Receptor Interactions. *Methods Mol Biol,* 2040**,** 41-50. 10.1007/978-1-4939-9686-5_3

Matthaeus, C., Lahmann, I., Kunz, S., Jonas, W., Melo, A. A., Lehmann, M., Larsson, E., Lundmark, R., Kern, M., Bluher, M., Olschowski, H., Kompa, J., Brugger, B., Muller, D. N., Haucke, V., Schurmann, A., Birchmeier, C. & Daumke, O. (2020). EHD2-mediated restriction of caveolar dynamics regulates cellular fatty acid uptake. *Proc Natl Acad Sci U S A,* 117**,** 7471-7481. 10.1073/pnas.1918415117

Matthaeus, C. & Taraska, J. W. (2020). Energy and Dynamics of Caveolae Trafficking. *Front Cell Dev Biol,* 8**,** 614472. 10.3389/fcell.2020.614472

Moren, B., Shah, C., Howes, M. T., Schieber, N. L., McMahon, H. T., Parton, R. G., Daumke, O. & Lundmark, R. (2012). EHD2 regulates caveolar dynamics via ATP-driven targeting and oligomerization. *Mol Biol Cell,* 23**,** 1316-29. 10.1091/mbc.E11-09-0787

Nishiumi, S. & Ashida, H. (2007). Rapid preparation of a plasma membrane fraction from adipocytes and muscle cells: application to detection of translocated glucose transporter 4 on the plasma membrane. *Biosci Biotechnol Biochem,* 71**,** 2343-6. 10.1271/bbb.70342

Nystrom, F. H., Chen, H., Cong, L. N., Li, Y. & Quon, M. J. (1999). Caveolin-1 interacts with the insulin receptor and can differentially modulate insulin signaling in transfected Cos-7 cells and rat adipose cells. *Mol Endocrinol,* 13**,** 2013-24. 10.1210/mend.13.12.0392

Park, S. Y., Ha, B. G., Choi, G. H., Ryu, J., Kim, B., Jung, C. Y. & Lee, W. (2004). EHD2 interacts with the insulin-responsive glucose transporter (GLUT4) in rat adipocytes and may participate in insulin-induced GLUT4 recruitment. *Biochemistry,* 43**,** 7552-62. 10.1021/bi049970f

Parpal, S., Karlsson, M., Thorn, H. & Stralfors, P. (2001). Cholesterol depletion disrupts caveolae and insulin receptor signaling for metabolic control via insulin receptor substrate-1, but not for mitogen-activated protein kinase control. *J Biol Chem,* 276**,** 9670-8. 10.1074/jbc.M007454200

Perona, J. S. (2017). Membrane lipid alterations in the metabolic syndrome and the role of dietary oils. *Biochim Biophys Acta Biomembr,* 1859**,** 1690-1703. 10.1016/j.bbamem.2017.04.015

Pohl, J., Ring, A., Korkmaz, U., Ehehalt, R. & Stremmel, W. (2005). FAT/CD36-mediated long-chain fatty acid uptake in adipocytes requires plasma membrane rafts. *Molecular Biology of the Cell,* 16**,** 24-31. 10.1091/mbc.E04-07-0616

Roccisana, J., Sadler, J. B., Bryant, N. J. & Gould, G. W. (2013). Sorting of GLUT4 into its insulin-sensitive store requires the Sec1/Munc18 protein mVps45. *Mol Biol Cell,* 24**,** 2389-97. 10.1091/mbc.E13-01-0011

Rodbell, M. (1964). Metabolism of Isolated Fat Cells. I. Effects of Hormones on Glucose Metabolism and Lipolysis. *J Biol Chem,* 239**,** 375-80.

Sadler, J. B., Roccisana, J., Virolainen, M., Bryant, N. J. & Gould, G. W. (2015). mVps45 knockdown selectively modulates VAMP expression in 3T3-L1 adipocytes. *Commun Integr Biol,* 8**,** e1026494. 10.1080/19420889.2015.1026494

Saito, T., Okada, S., Nohara, A., Tagaya, Y., Osaki, A., Oh, I. S., Takahashi, H., Tsuchiya, T., Hashimoto, K., Satoh, T., Yamada, M., Pessin, J. E. & Mori, M. (2012). Syntaxin4 interacting protein (Synip) binds phosphatidylinositol (3,4,5) triphosphate. *PLoS One,* 7**,** e42782. 10.1371/journal.pone.0042782

Salaun, C., Gould, G. W. & Chamberlain, L. H. (2005). Lipid raft association of SNARE proteins regulates exocytosis in PC12 cells. *J Biol Chem,* 280**,** 19449-53. 10.1074/jbc.M501923200

Schnitzer, J. E., Liu, J. & Oh, P. (1995). Endothelial caveolae have the molecular transport machinery for vesicle budding, docking, and fusion including VAMP, NSF, SNAP, annexins, and GTPases. *J Biol Chem,* 270**,** 14399-404. 10.1074/jbc.270.24.14399

Sezgin, E., Levental, I., Mayor, S. & Eggeling, C. (2017). The mystery of membrane organization: composition, regulation and roles of lipid rafts. *Nat Rev Mol Cell Biol,* 18**,** 361-374. 10.1038/nrm.2017.16

Stoeber, M., Stoeck, I. K., Hanni, C., Bleck, C. K., Balistreri, G. & Helenius, A. (2012). Oligomers of the ATPase EHD2 confine caveolae to the plasma membrane through association with actin. *EMBO J,* 31**,** 2350-64. 10.1038/emboj.2012.98

Stralfors, P. (2012). Caveolins and caveolae, roles in insulin signalling and diabetes. *Adv Exp Med Biol,* 729**,** 111-26. 10.1007/978-1-4614-1222-9_8

Suresh, P., Miller, W. T. & London, E. (2021). Phospholipid exchange shows insulin receptor activity is supported by both the propensity to form wide bilayers and ordered raft domains. *J Biol Chem,* 297**,** 101010. 10.1016/j.jbc.2021.101010

Takeda, H., Izumi, Y., Takahashi, M., Paxton, T., Tamura, S., Koike, T., Yu, Y., Kato, N., Nagase, K., Shiomi, M. & Bamba, T. (2018). Widely-targeted quantitative lipidomics method by supercritical fluid chromatography triple quadrupole mass spectrometry. *J Lipid Res,* 59**,** 1283-1293. 10.1194/jlr.D083014

Thorn, H., Stenkula, K. G., Karlsson, M., Ortegren, U., Nystrom, F. H., Gustavsson, J. & Stralfors, P. (2003). Cell surface orifices of caveolae and localization of caveolin to the necks of caveolae in adipocytes. *Mol Biol Cell,* 14**,** 3967-76. 10.1091/mbc.e03-01-0050

Vainio, S., Heino, S., Mansson, J. E., Fredman, P., Kuismanen, E., Vaarala, O. & Ikonen, E. (2002). Dynamic association of human insulin receptor with lipid rafts in cells lacking caveolae. *EMBO Rep,* 3**,** 95-100. 10.1093/embo-reports/kvf010

Wang, C., Tu, J., Zhang, S., Cai, B., Liu, Z., Hou, S., Zhong, Q., Hu, X., Liu, W., Li, G., Liu, Z., He, L., Diao, J., Zhu, Z. J., Li, D. & Liu, C. (2020). Different regions of synaptic vesicle membrane regulate VAMP2 conformation for the SNARE assembly. *Nat Commun,* 11**,** 1531. 10.1038/s41467-020-15270-4

Wang, T., Li, L. & Hong, W. (2017). SNARE proteins in membrane trafficking. *Traffic,* 18**,** 767-775. 10.1111/tra.12524

Yamamoto, M., Toya, Y., Schwencke, C., Lisanti, M. P., Myers, M. G., Jr. & Ishikawa, Y. (1998). Caveolin is an activator of insulin receptor signaling. *J Biol Chem,* 273**,** 26962-8. 10.1074/jbc.273.41.26962

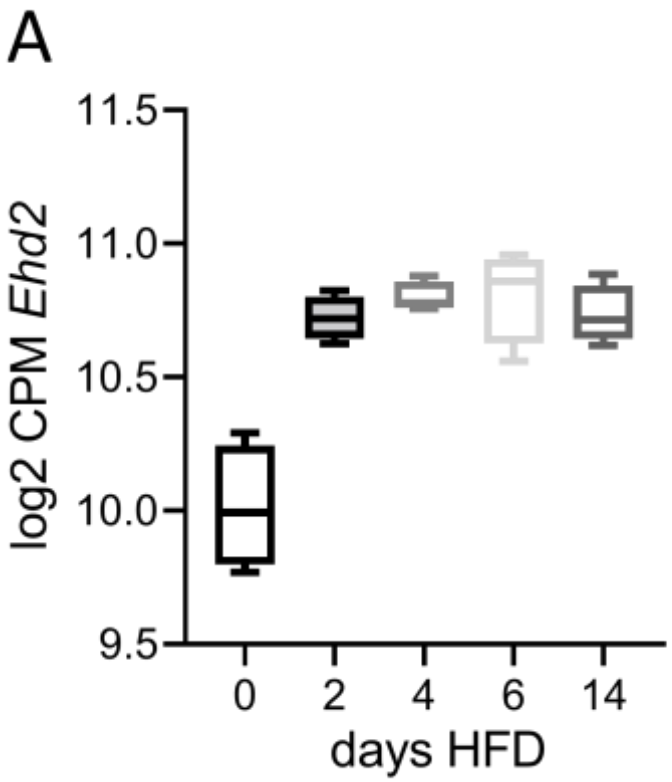
A
11.5
11.0
10.5
10.0
9.5
log2 CPM Ehd2
0
2
4
6
14
days HFD

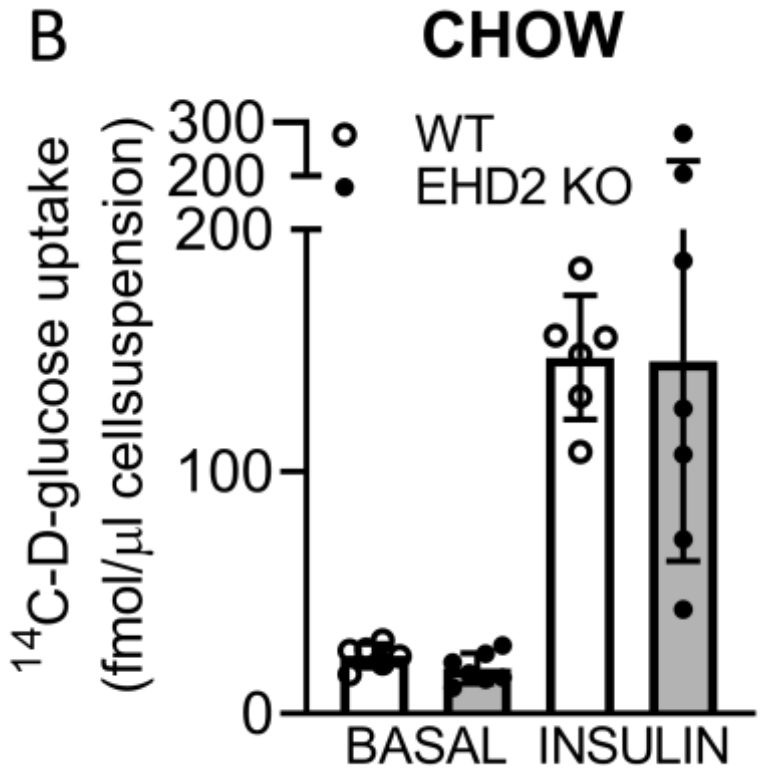
B
CHOW
300
200
200
100
0
WT
EHD2 KO
14C-D-glucose uptake
(fmol/µl cellsuspension)
BASAL
INSULIN

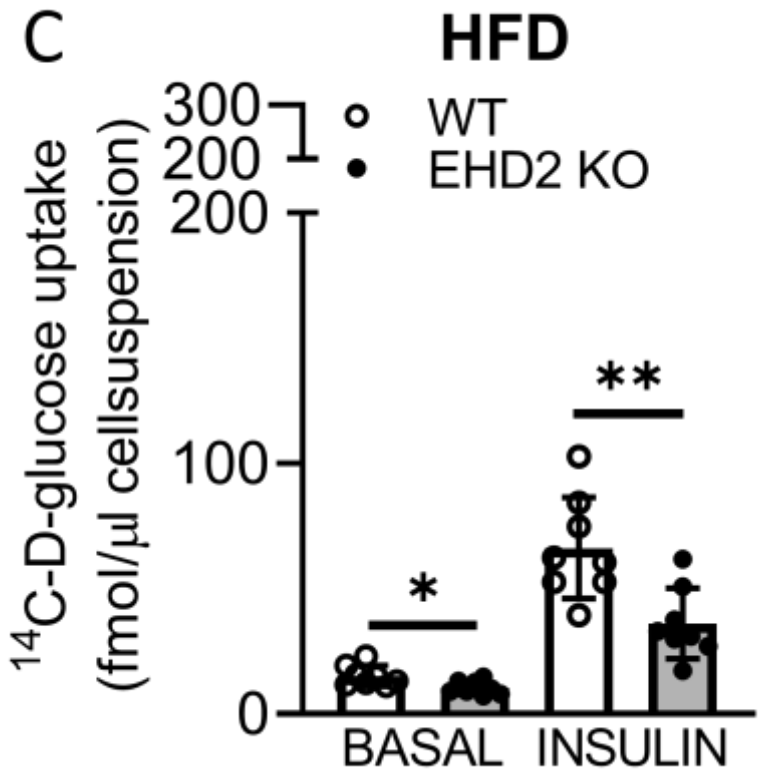
C
HFD
WT
EHD2 KO
^{14}C-D-glucose uptake
(fmol/µl cellsuspension)
300
200
200
100
0
*
**
BASAL
INSULIN

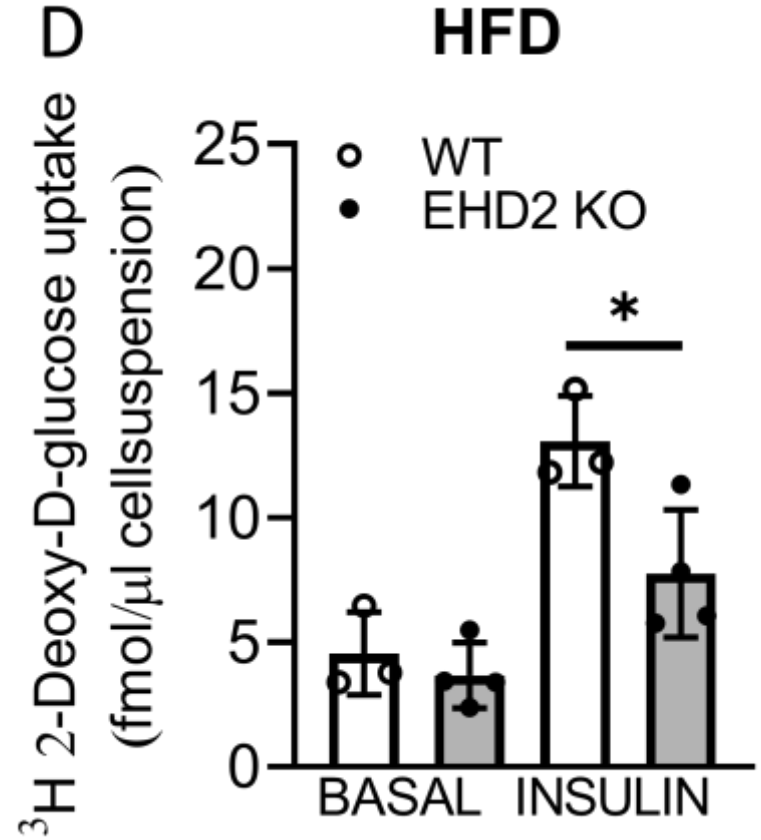
D
HFD
WT
EHD2 KO
^{3}H 2-Deoxy-D-glucose uptake
(fmol/µl cellsuspension)
25
20
15
10
5
0
*
BASAL
INSULIN

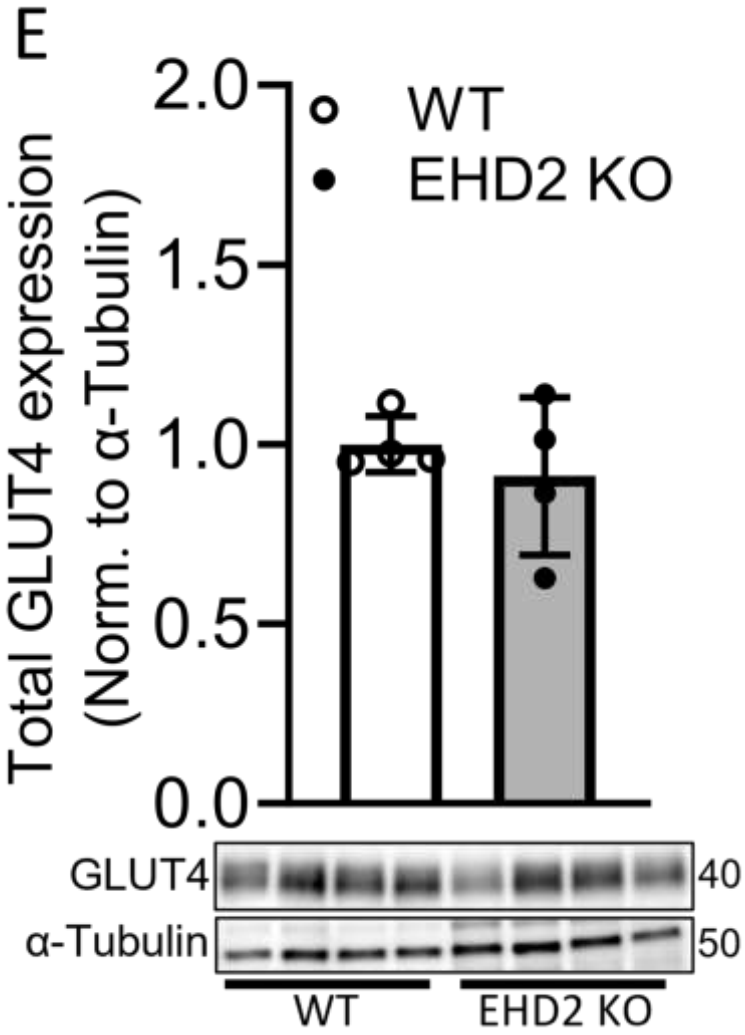
E
Total GLUT4 expression
(Norm. to α-Tubulin)
2.0
1.5
1.0
0.5
0.0
WT
EHD2 KO
GLUT4
α-Tubulin
40
50
WT
EHD2 KO

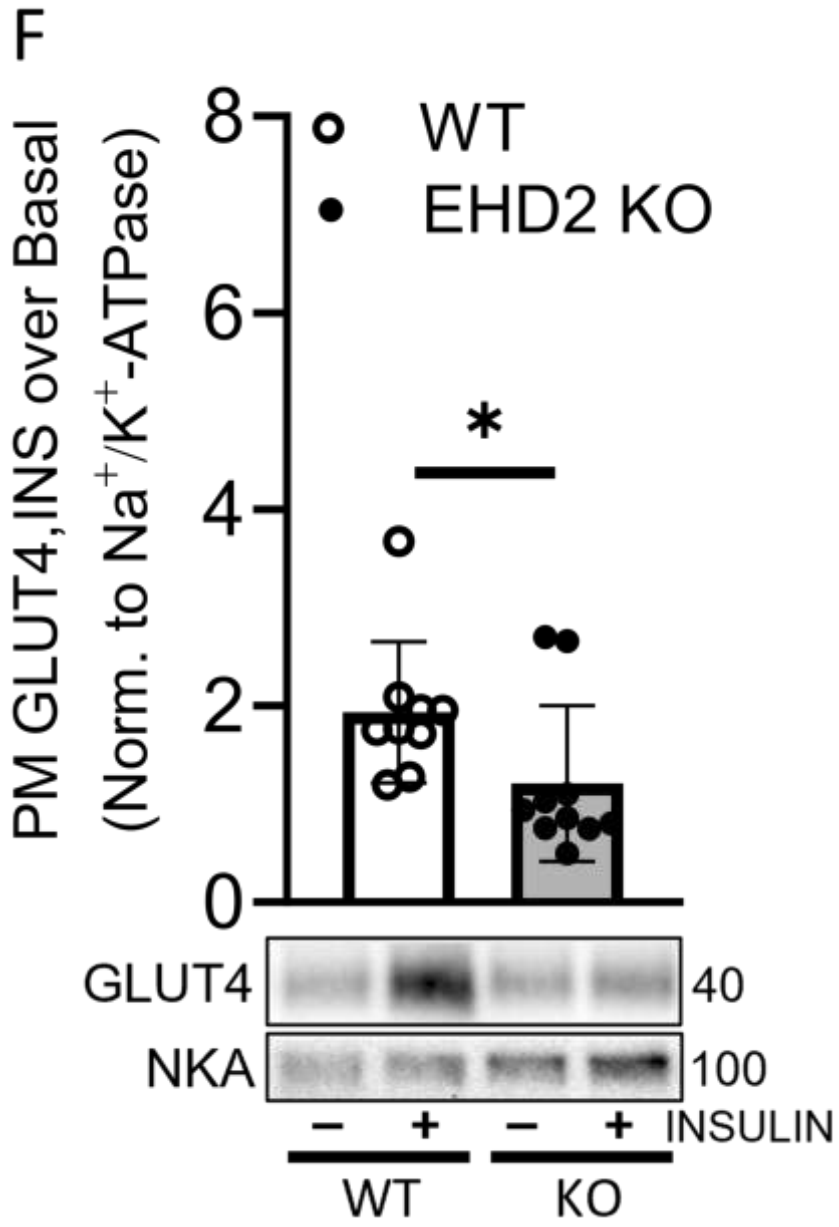
F
PM GLUT4,INS over Basal
(Norm. to Na+/K+-ATPase)
8
6
4
2
0
WT
EHD2 KO
*
GLUT4
NKA
40
100
– + – + INSULIN
WT
KO

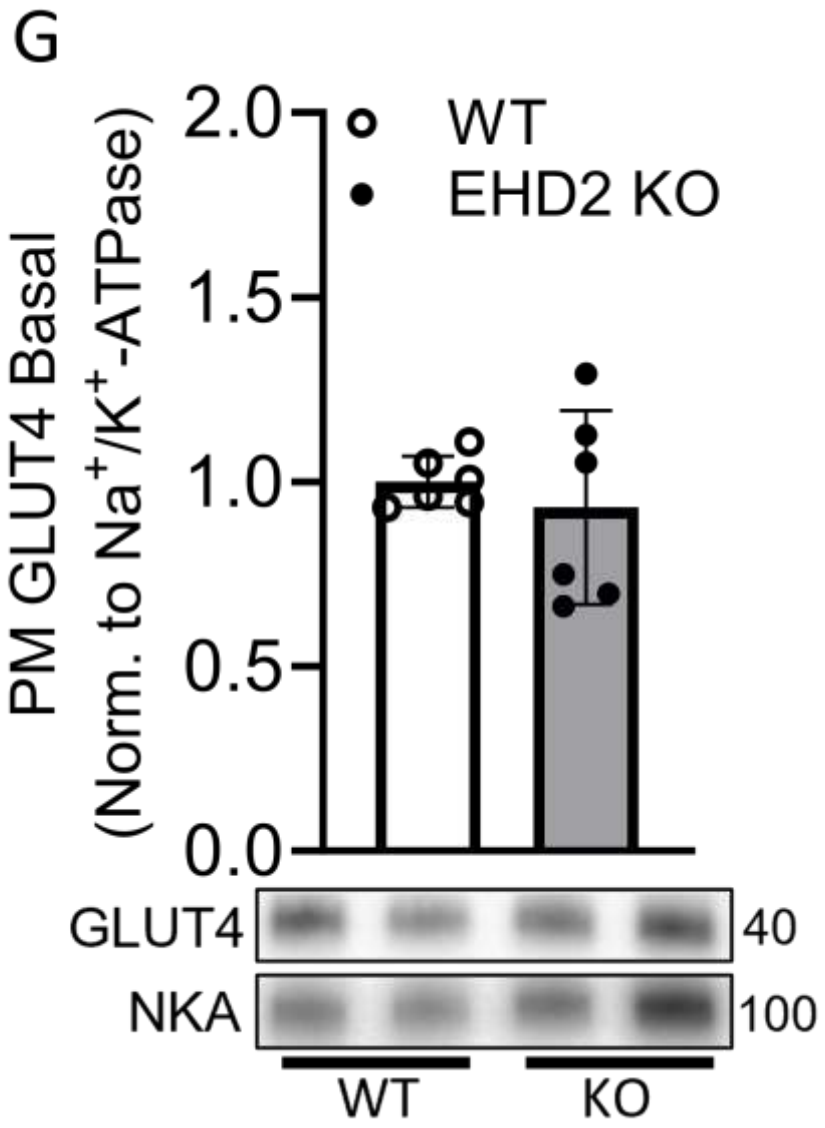
G
PM GLUT4 Basal
(Norm. to Na+/K+-ATPase)
2.0
1.5
1.0
0.5
0.0
WT
EHD2 KO
GLUT4
NKA
40
100
WT
KO

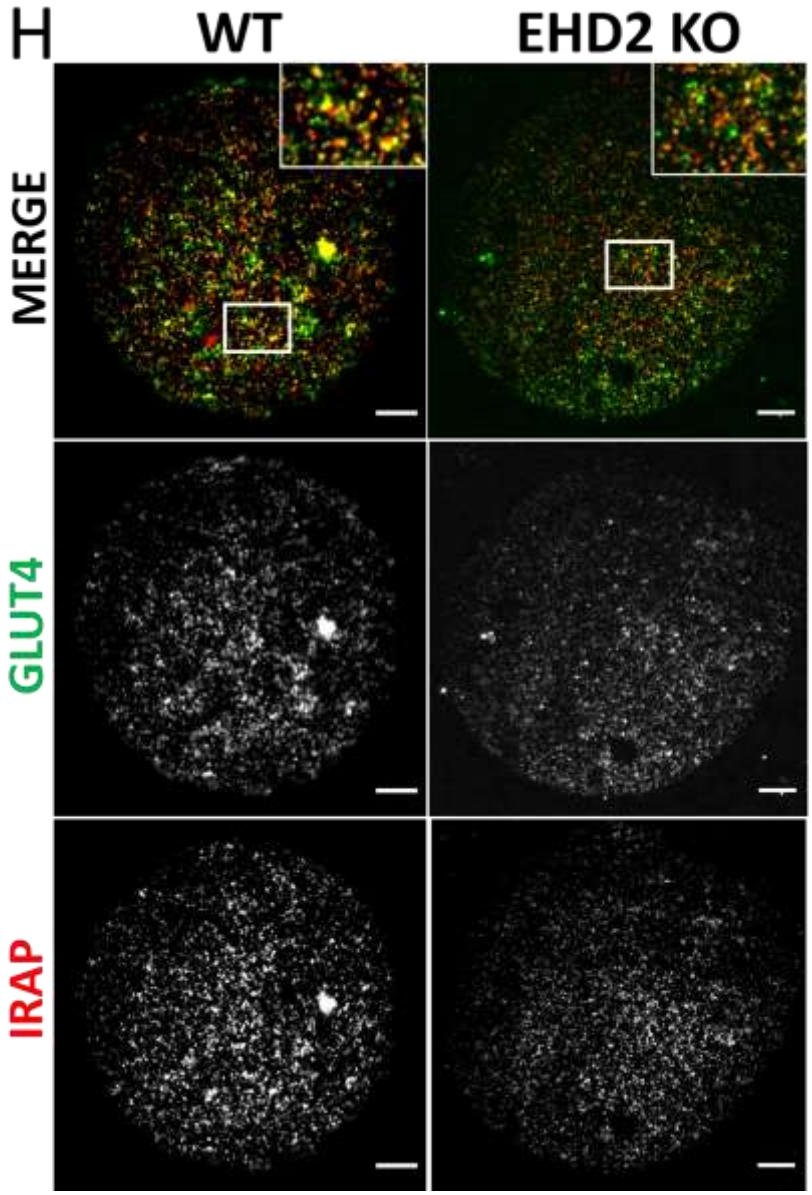
WT
EHD2 KO
MERGE
GLUT4
IRAP

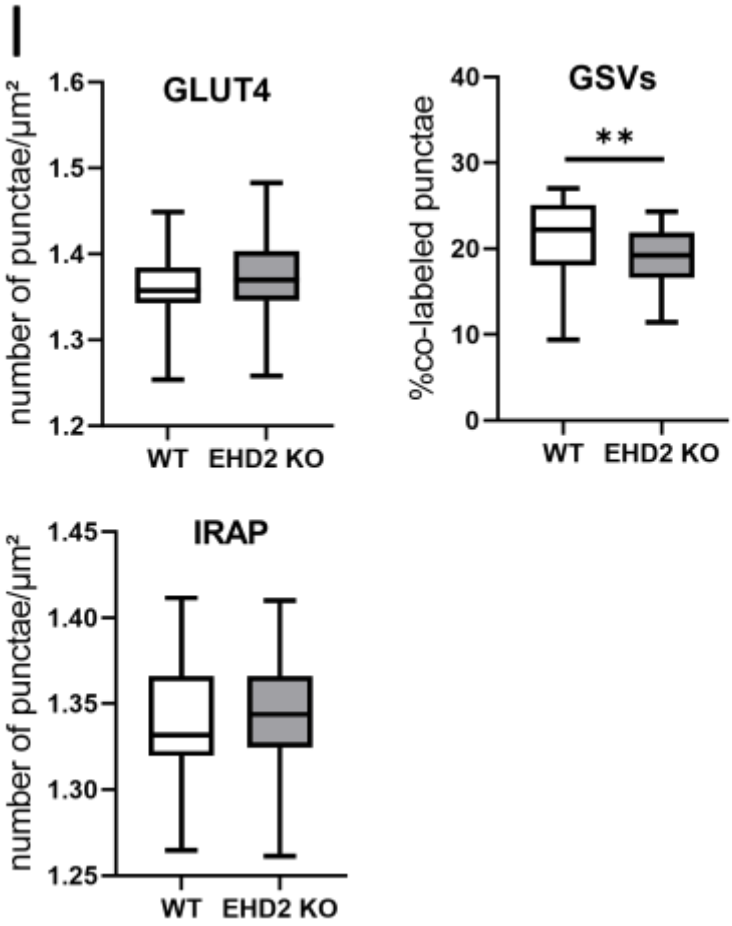

Figure legends

Figure 1. Insulin-stimulated glucose uptake and GLUT4 dynamics of EHD2 deficient adipocytes

(A) RNA expression of *Ehd2* at day 0 (chow), 2, 4, 6 and 14 days of HFD in epididymal adipose tissue. Average expression of n=4 per group is displayed in log 'counts per million'. (B-I) refers to data collected from primary inguinal adipocytes isolated from WT and EHD2 KO mice. Non (basal) and insulin-stimulated (1 nM, 30 min) glucose uptake in primary inguinal adipocytes isolated from chow-fed (B) or HFD-fed (C) mice using ^{14}C-glucose tracer assay, n=6-8 biological replicates. (D) [3H]2-Deoxy-d-glucose (2-DG) uptake in non (basal) and insulin-stimulated (1 nM, 30 min) from HFD-fed mice, n=3-4 biological replicates. (E) GLUT4 protein levels in non-stimulated whole cell lysates; each lane representates a biological replicate, n=4. (F) Insulin-stimulated (1 nM, 30 min) GLUT4 translocation in HFD inguinal adipocytes using plasma membrane sedimentation assay (Nishiumi and Ashida, 2007). Data are displayed as fold change of insulin over basal. n=9-10, statistical comparison was carried out using Mann Whitney test *p≤0.05. (G) GLUT4 protein levels in non-stimulated (basal) plasma membrane fractions, n=5 biological replicates. (H) Representative

TIRF images of inguinal adipocytes isolated from wildtype and EHD2 KO mice; (35 cells/replicate). Scale bar=10 µm. Cells were co-labeled with GLUT4 (green) and IRAP (red) antibodies. (I) Number of GLUT4 positive punctae/μm^2, number of IRAP positive punctae/μm^2 and quantification of co-labeled punctae (GLUT4 and IRAP) below 140 nm, expressed as percentage of all detected GLUT4 puncta (defined as GSVs). If not stated otherwise, unpaired two-samples t-test was used for statistical analysis. Data are displayed as mean±SD and significance was determined according to *$p \leq 0.05$ and **$p \leq 0.01$. All displayed results, except for (A) and (B), were obtained from inguinal adipocytes after 2 weeks of HFD. NKA= Na^+/K^+-ATPase.

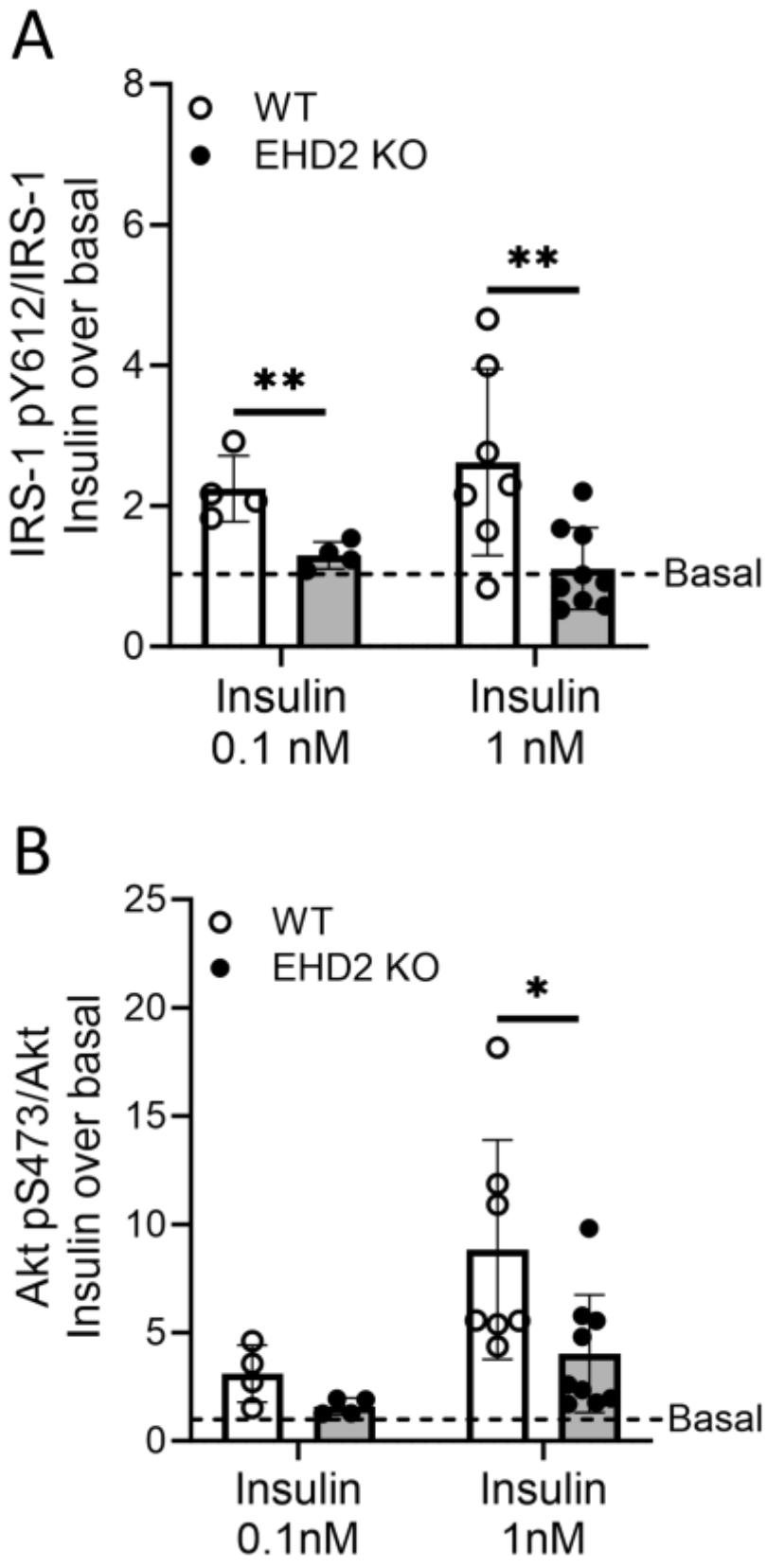
A
IRS-1 pY612/IRS-1
Insulin over basal
WT
EHD2 KO
**
**
Basal
Insulin
0.1 nM
Insulin
1 nM
B
Akt pS473/Akt
Insulin over basal
WT
EHD2 KO
*
Basal
Insulin
0.1nM
Insulin
1nM

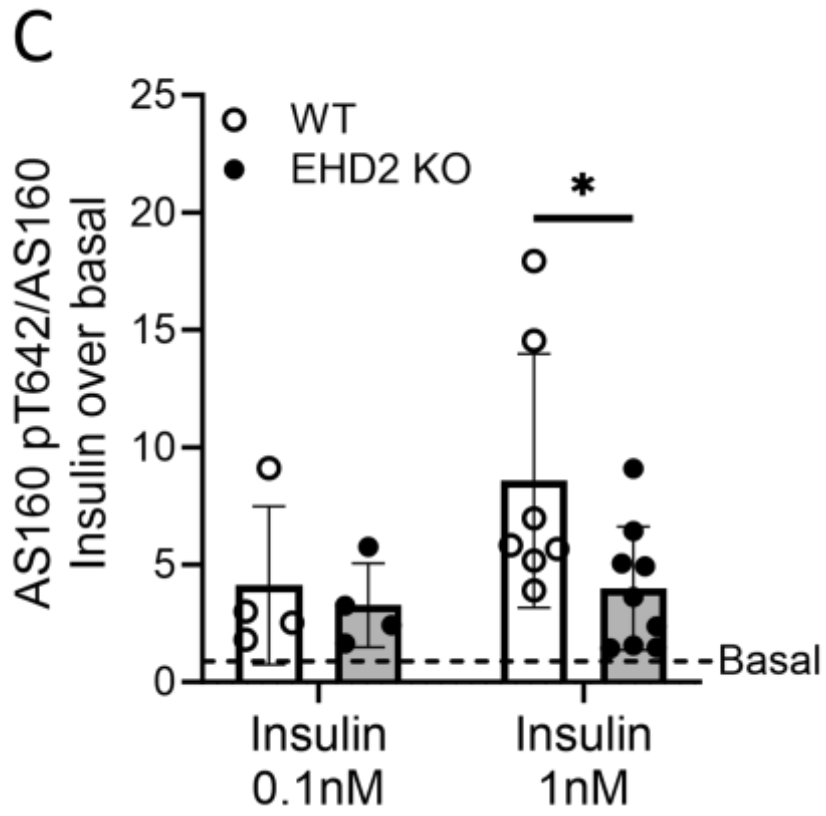
C
AS160 pT642/AS160
Insulin over basal
25
20
15
10
5
0
WT
EHD2 KO
*
Basal
Insulin
0.1nM
Insulin
1nM

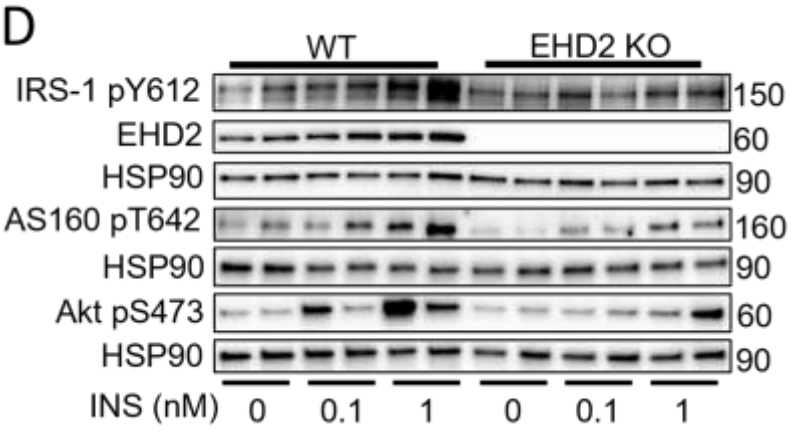
D
WT
EHD2 KO
IRS-1 pY612
EHD2
HSP90
AS160 pT642
HSP90
Akt pS473
HSP90
150
60
90
160
90
60
90
INS (nM) 0 0.1 1 0 0.1 1

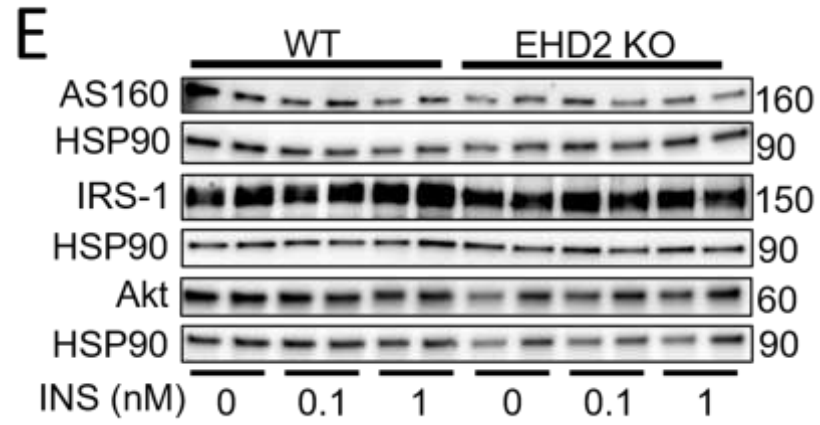
E
WT
EHD2 KO
AS160
HSP90
IRS-1
HSP90
Akt
HSP90
160
90
150
90
60
90
INS (nM) 0 0.1 1 0 0.1 1

Figure 2. Impaired insulin signalling in EHD2 KO adipocytes

Inguinal adipocytes were non-stimulated or stimulated with insulin (0.1 or 1 nM) for 30 min, followed by western blot analysis to detect total and phosphorylated protein levels of (A) IRS-1 (pY612), (B) AKT (pS473), (C) AS160 (pT642) and EHD2. Data are presented as fold change of insulin over basal (basal=1, displayed as dashed line). Representative western blots of phosphorylated protein levels (D) and total protein levels (E) of two biological replicates. Basal (phosphorylated/total) protein levels are available in Supplement Figure S1B. Data are displayed as mean±SD. Statistical comparison was carried out using using Mann Whitney test (1nM Akt S473 and 1nM AS160 Thr642) or unpaired two-sample t-test. Significance was determined according to *$p \leq 0.05$ and **$p \leq 0.01$. Representative blots from n =4-9 biological replicates. All displayed results were obtained from inguinal adipocytes 2 weeks of HFD.

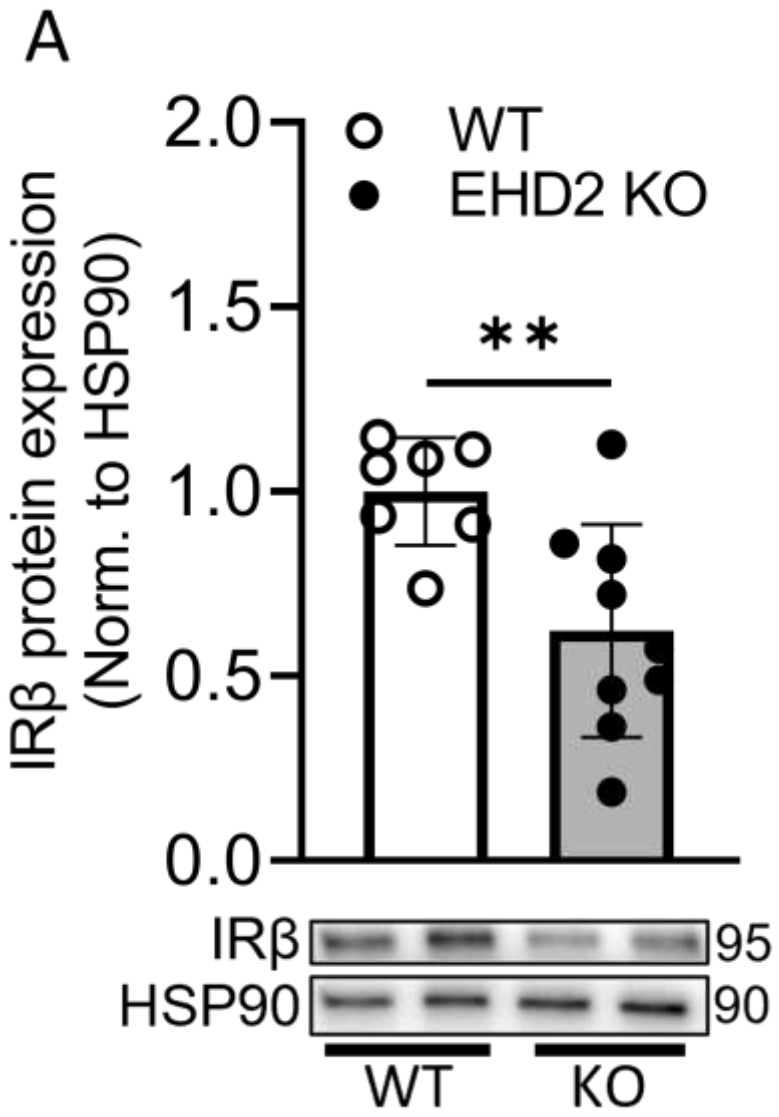
A
2.0
1.5
1.0
0.5
0.0
WT
EHD2 KO
**
IRβ protein expression
(Norm. to HSP90)
IRβ
HSP90
95
90
WT
KO

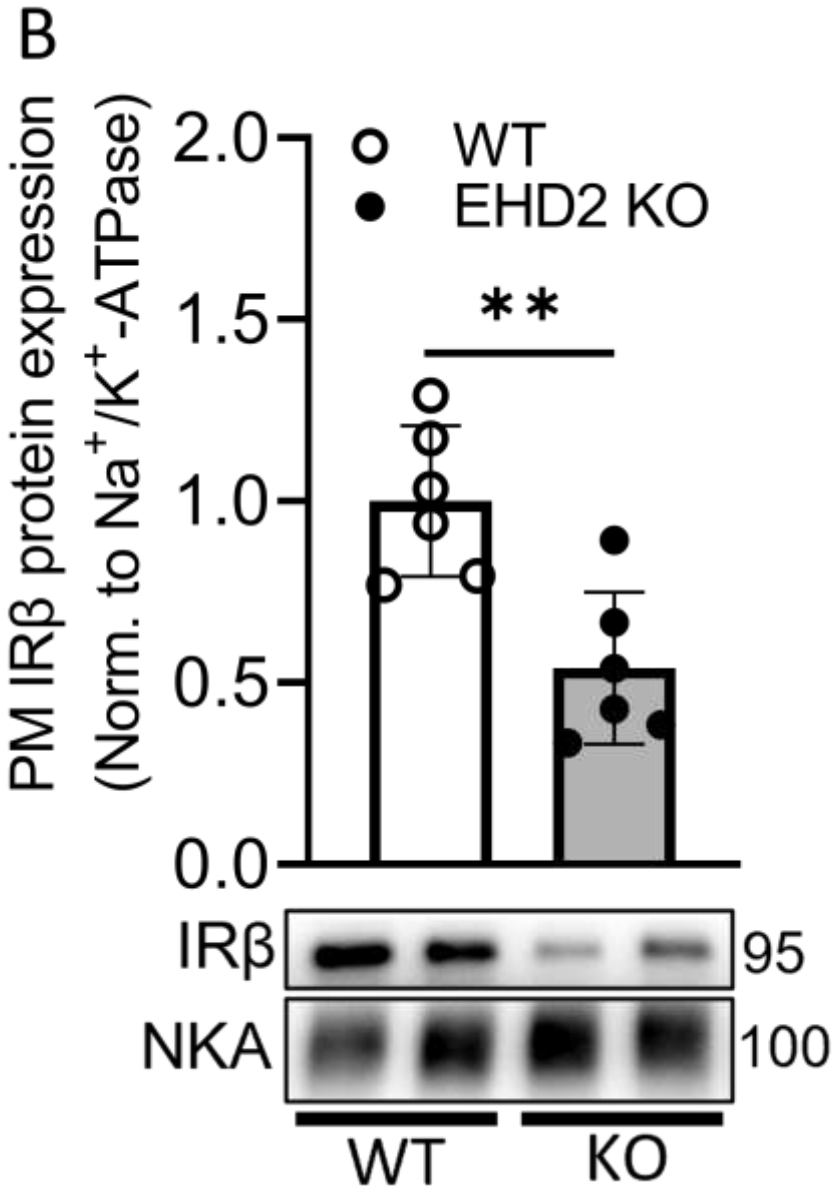
B
PM IRβ protein expression
(Norm. to Na+/K+-ATPase)
2.0
1.5
1.0
0.5
0.0
WT
EHD2 KO
**
IRβ
NKA
95
100
WT
KO

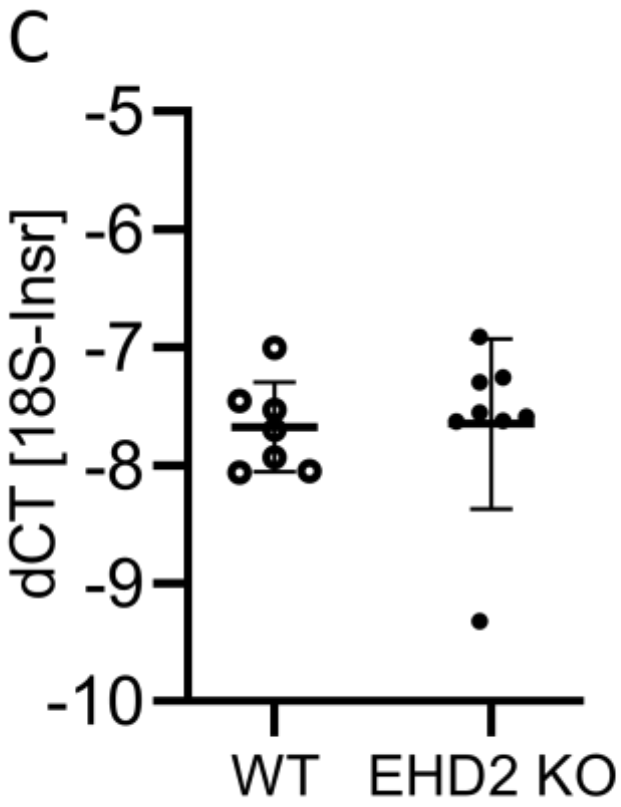
C
dCT [18S-Insr]
-5
-6
-7
-8
-9
-10
WT
EHD2 KO

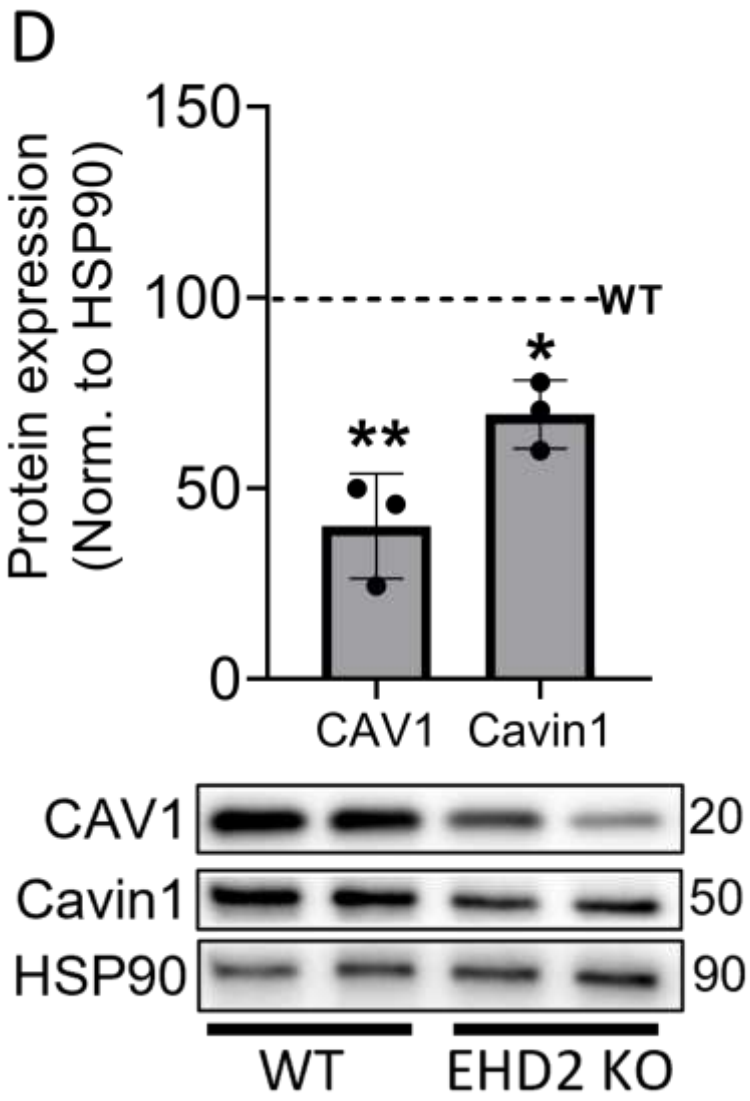
D
Protein expression
(Norm. to HSP90)
150
100
50
0
WT
**
*
CAV1
Cavin1
CAV1
Cavin1
HSP90
20
50
90
WT
EHD2 KO

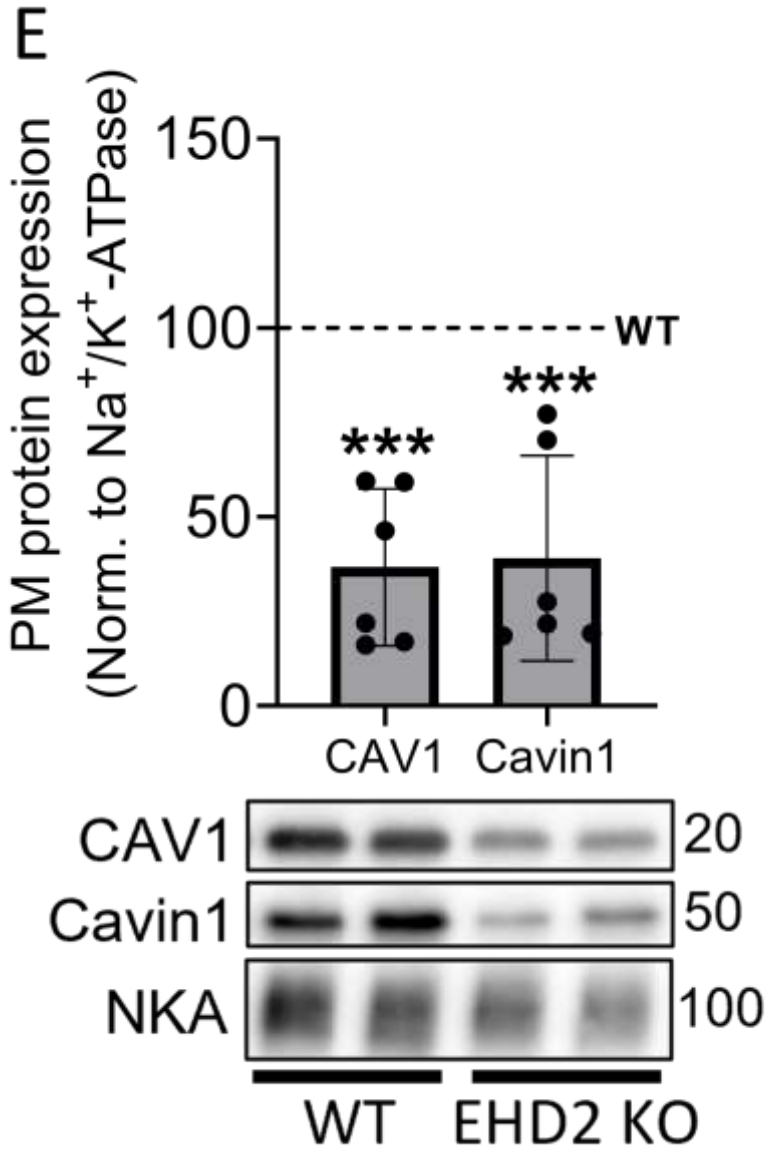
E
PM protein expression
(Norm. to Na+/K+-ATPase)
150
100
50
0
WT
***
***
CAV1
Cavin1
CAV1
Cavin1
NKA
20
50
100
WT
EHD2 KO

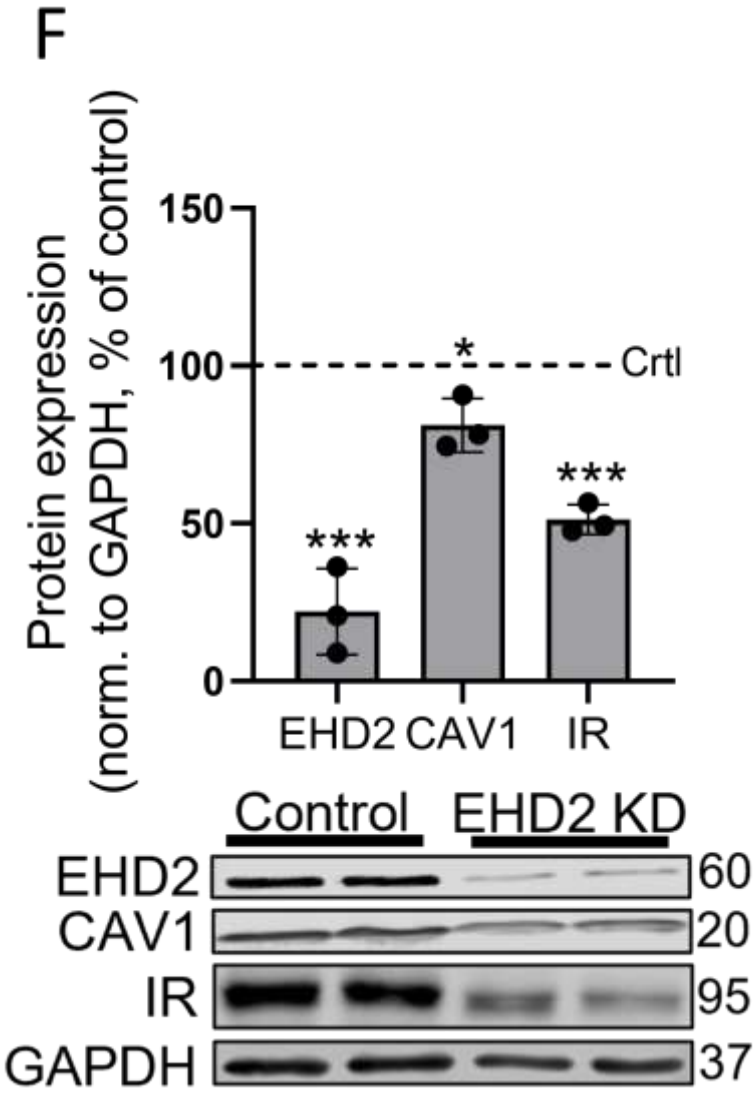
F
Protein expression
(norm. to GAPDH, % of control)
150
100
50
0
Crtl
*
***
***
EHD2
CAV1
IR
Control
EHD2 KD
EHD2
CAV1
IR
GAPDH
60
20
95
37

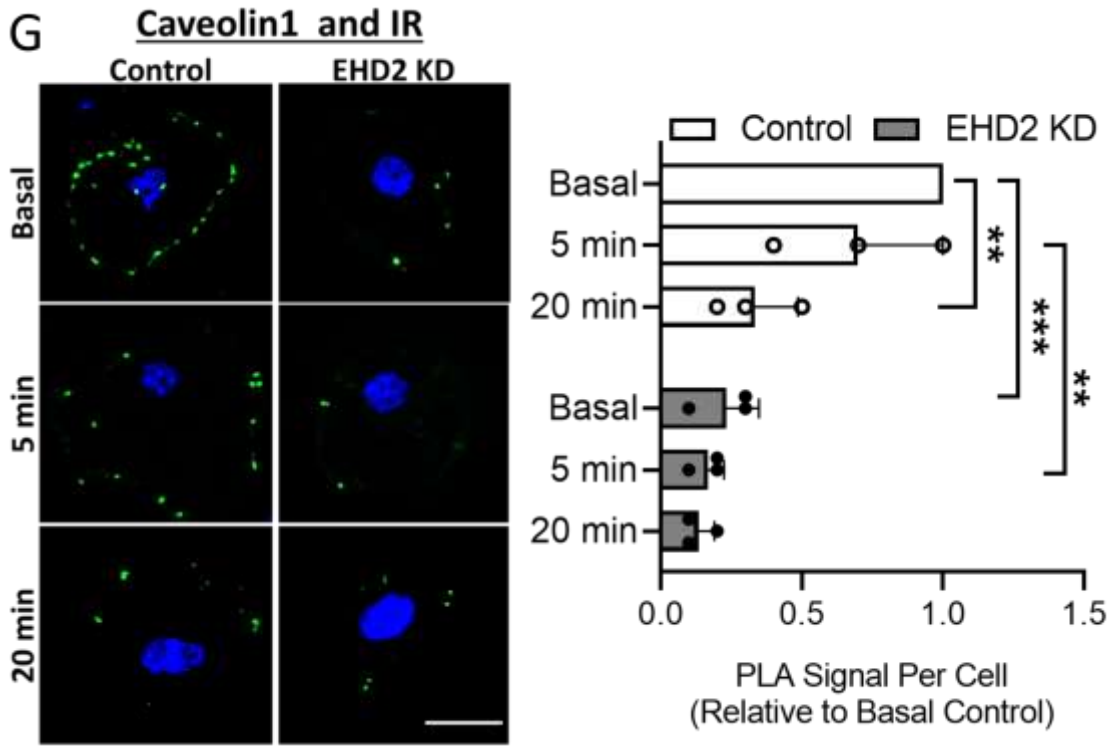

Figure 3. Impaired insulin receptor stability and blunted CAV1/IRbeta interaction in EHD2 KO adipocytes

Protein levels of insulin receptor beta (IRβ) in whole-cell (A) and plasma membrane (B). Data are displayed as mean±SD and normalized to WT proteins levels. (A) n=7-8 biological replicates and (B) n=6 biological replicates/condition. (C) RNA was isolated from inguinal adipose tissue, and insulin receptor gene expression was examined using qPCR. Statistical analysis carried out on dCT values, and dCT was calculated as $dCT=CT_{ref} - CT_{goi}$, n=7-8 biological replicates. Whole-cell (D) and plasma membrane (E) caveolin-1 and cavin1 protein levels in primary adipocytes. Data are displayed as % of WT levels (WT=100%, dashed line); n=3 biological replicates/condition (D), n=5-6 biological replicates (E). (F) Protein expression of EHD2, caveolin-1 and insulin receptor beta normalized to GAPDH in 3T3-L1 adipocytes of either control siRNA or EHD2 siRNA cells. Data are displayed as % of control levels (control=100%, dashed line), n=3 biological replicates. Statistical analysis was carried out using unpaired two-sample t-test. Significance was determined according to *p≤0.05, **p≤0.01, ***p≤0.001. (G) Proximity Ligation Assay (PLA) was used to quantify the interaction of caveolin-1 and IRβ in 3T3-L1 adipocytes, fixed 96 h after gene silencing with control siRNA (Control) or EHD2 siRNA (EHD2 KD), and following 0 (Basal), 5 or 20 min stimulation with 100 nM insulin. Representative images, with PLA signal in green and nuclei staining (DAPI) in blue are shown alongside corresponding quantification of PLA signal per cell normalized to Basal Control. Mean±SD of n=3 independent experiments are shown. Statistical analysis was done using two-way ANOVA, Tukey's Honestly-Significant-Difference (TukeyHSD) , *p<0.05, **p<0.01, ***p<0.001. Scale bar=10 µm. NKA= Na^+/K^+-ATPase.

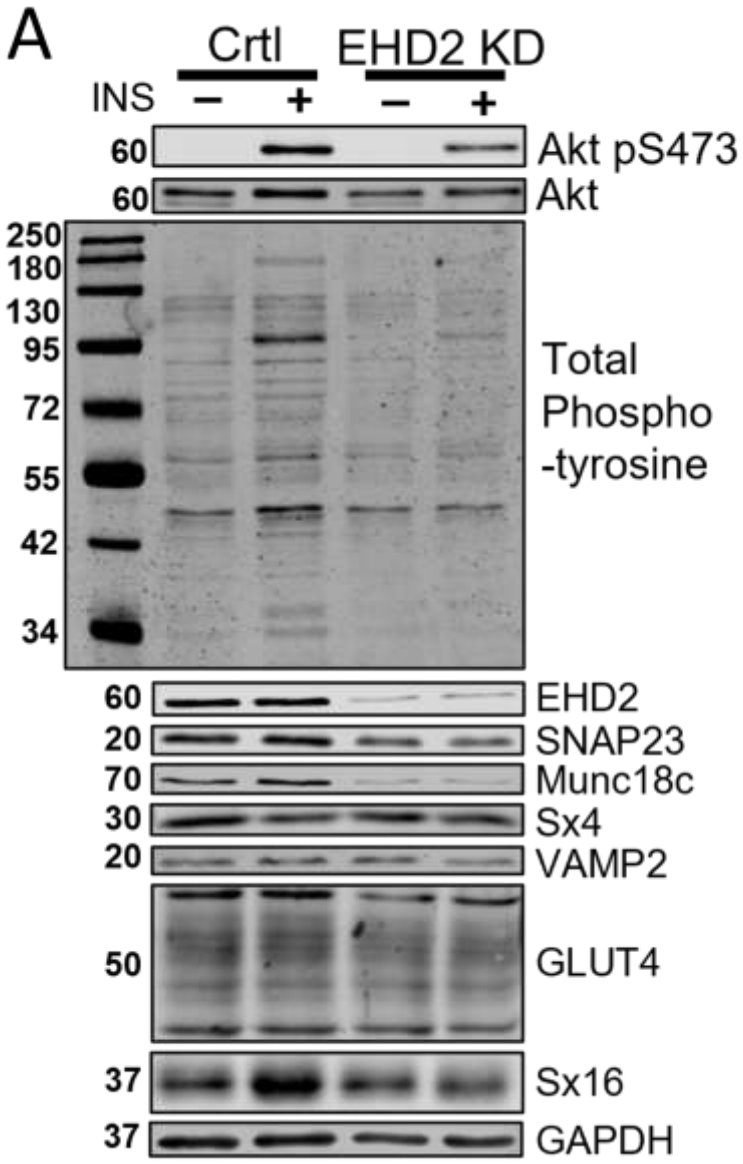
A
Crtl
EHD2 KD
INS
–
+
–
+
60
Akt pS473
60
Akt
250
180
130
95
72
55
42
34
Total
Phospho
-tyrosine
60
EHD2
20
SNAP23
70
Munc18c
30
Sx4
20
VAMP2
50
GLUT4
37
Sx16
37
GAPDH

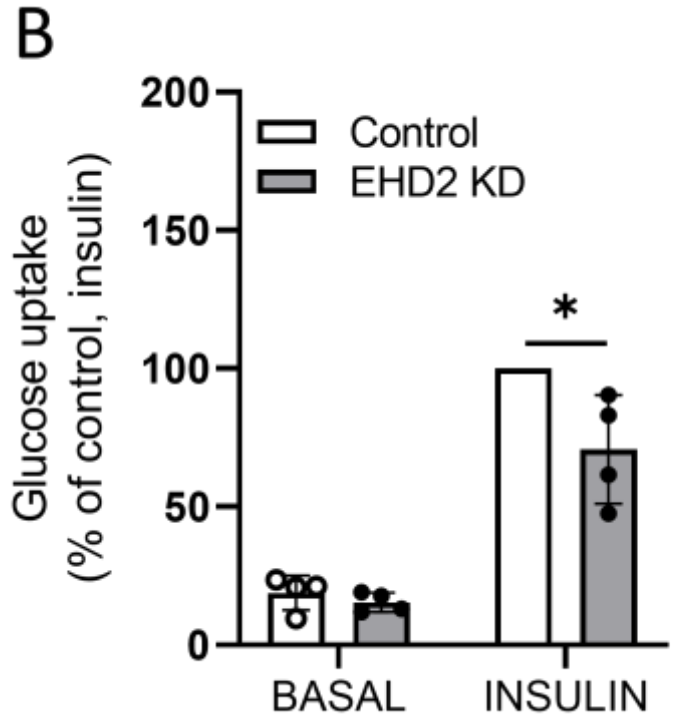

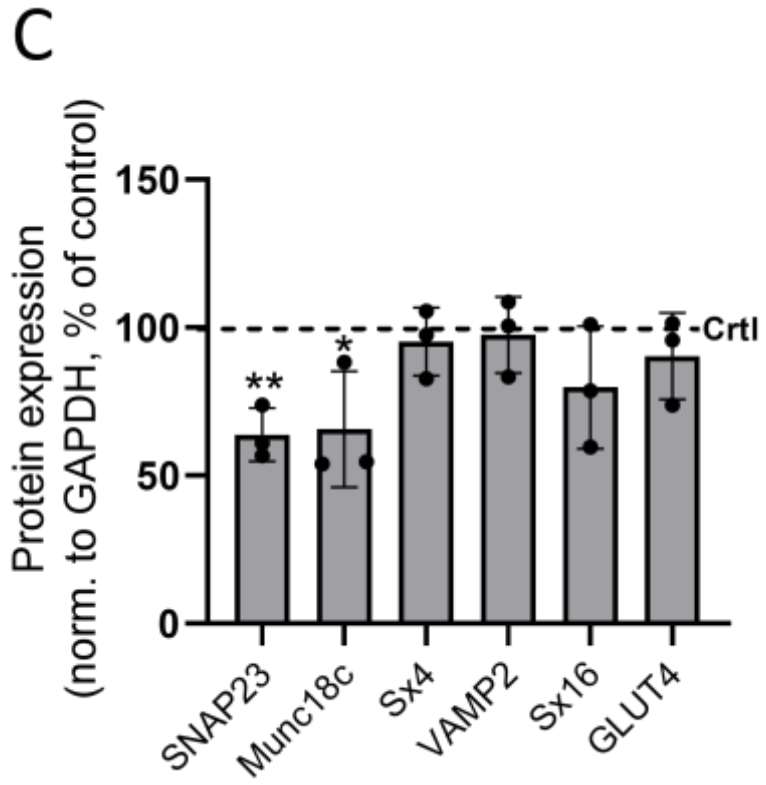

Figure 4. EHD2 knockdown in 3T3-L1 adipocytes is associated with impaired insulin signalling

(A) Representative western blots of total phospho-tyrosine in 3T3-L1 adipocyte lysates collected 96 h after gene silencing with control siRNA or EHD2 siRNA, either untreated or

following 20 min stimulation with 100 nM insulin (n=2) and of protein levels of EHD2, SNARE proteins Syntaxin4 (Sx4), SNAP23, VAMP2 and Syntaxin16 (Sx16), as well as regulatory protein Munc18c, and GLUT4 (n=3). GAPDH was used as a loading control and the calculations displayed in (C) were performed exclusively on basal samples. (B) Glucose uptake (2-deoxy-D-glucose) of 3T3-L1 adipocytes, 96 h after gene silencing with control siRNA (Control) or EHD2 siRNA (EHD2 KD), with (INS) or without (Basal) 20 min stimulation with 100 nM insulin. Data were corrected for non-specific cellular isotope uptake by performing parallel assays in the presence of 10 µM cytochalasin B and normalized to those obtained in the insulin-stimulated control adipocytes for each data set. Mean±SD of n=4 independent experiments are shown. Statistical analysis was done using two-way ANOVA Tukey's Honestly-Significant-Difference (TukeyHSD), *p< 0.05. (C) Corresponding quantification of protein expression in EHD2 siRNA knockdown adipocytes in the absence of an acute insulin challenge (lanes labelled '-' in (A)) is normalized to GAPDH and expressed as a percentage of protein expression in control siRNA adipocytes. Mean and SD of n=3 independent experiments are shown. Statistical analysis was conducted using unpaired two-sample t-test, *p <0.05, **p<0.01, ***p<0.001.

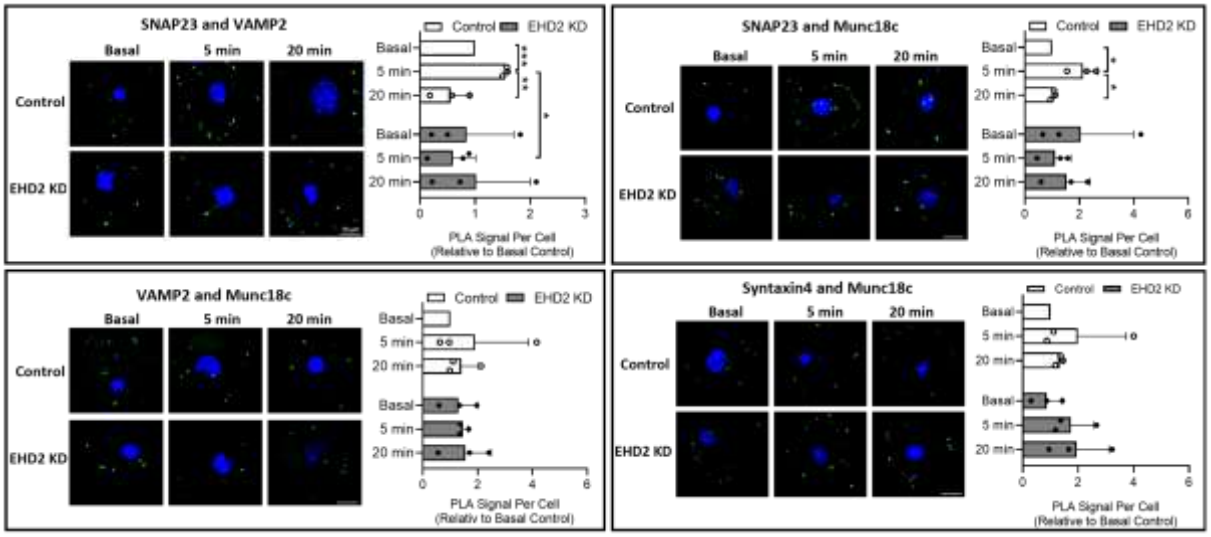

Figure 5. EHD2 KD in 3T3-L1 adipocytes causes impaired SNARE protein assembly

Proximity Ligation Assay (PLA) was used to assess pairwise interactions of proteins in 3T3-L1 adipocytes, fixed 96 h after gene silencing with control siRNA (Control) or EHD2 siRNA (EHD2 KD), and following 0 (Basal), 5 or 20 min stimulation with 100 nM insulin. Representative images, with PLA signal in green and nuclei staining (DAPI) in blue are shown alongside corresponding quantification of PLA signal per cell normalized to Basal Control for the following protein pairs: (A) SNAP23 and VAMP2; (B) SNAP23 and Munc18c; (C) VAMP2 and Munc18c and (D) Syntaxin4 and Munc18c. Mean±SD of n=3 independent experiments are shown. Quantification was performed in ImageJ, and statistical analysis was done using two-way ANOVA, Tukey's Honestly-Significant-Difference (TukeyHSD), *p<0.05, **p<0.01, ***p<0.001. Scale bar=10 µm.

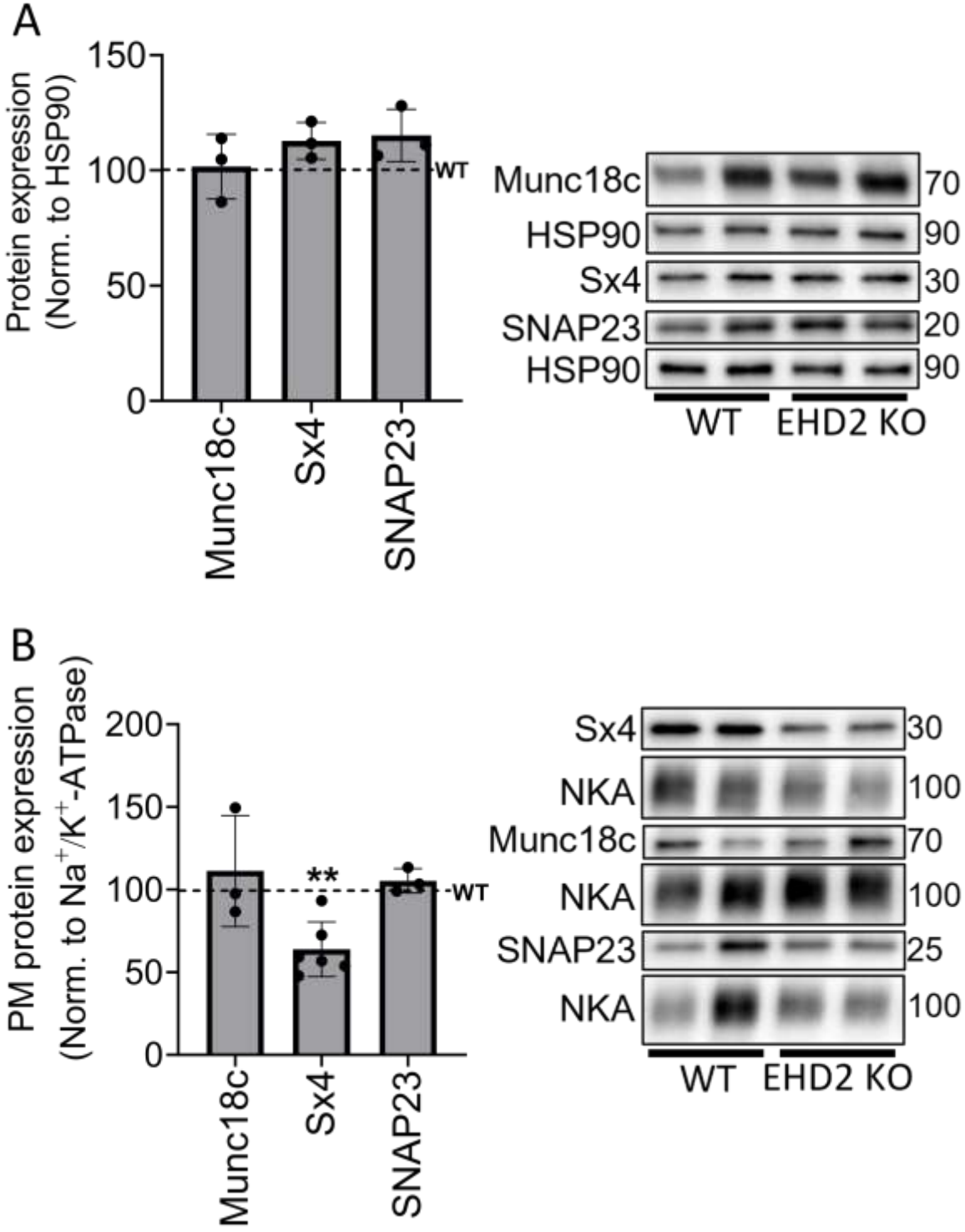
A
Protein expression
(Norm. to HSP90)
150
100
50
0
WT
Munc18c
Sx4
SNAP23
Munc18c
HSP90
Sx4
SNAP23
HSP90
70
90
30
20
90
WT
EHD2 KO
B
PM protein expression
(Norm. to Na+/K+-ATPase)
200
150
100
50
0
**
WT
Munc18c
Sx4
SNAP23
Sx4
NKA
Munc18c
NKA
SNAP23
NKA
30
100
70
100
25
100
WT
EHD2 KO

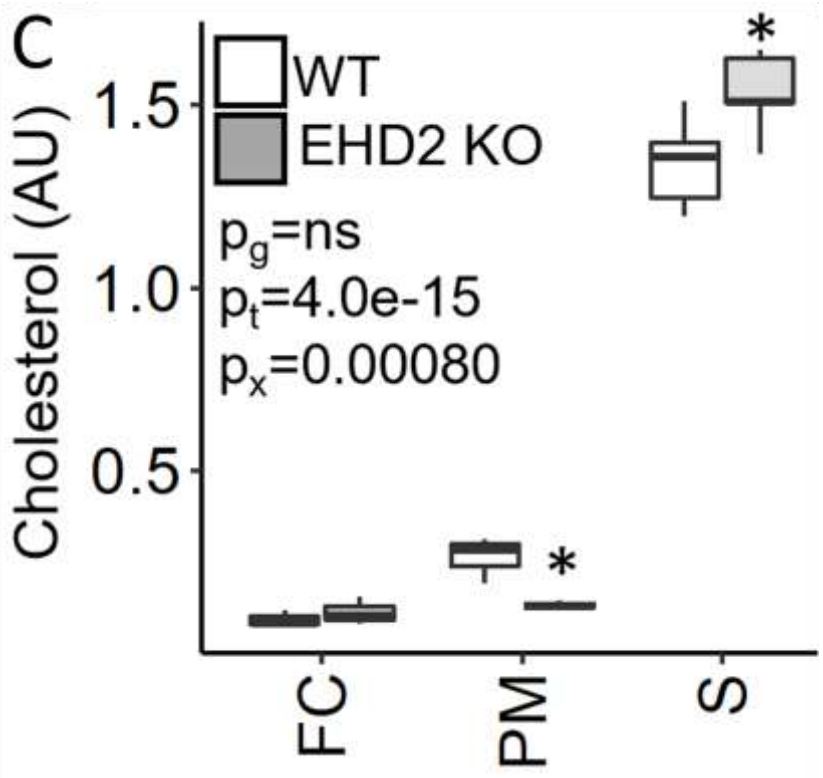
C
Cholesterol (AU)
1.5
1.0
0.5
WT
EHD2 KO
p_g=ns
p_t=4.0e-15
p_x=0.00080
*
*
FC
PM
S

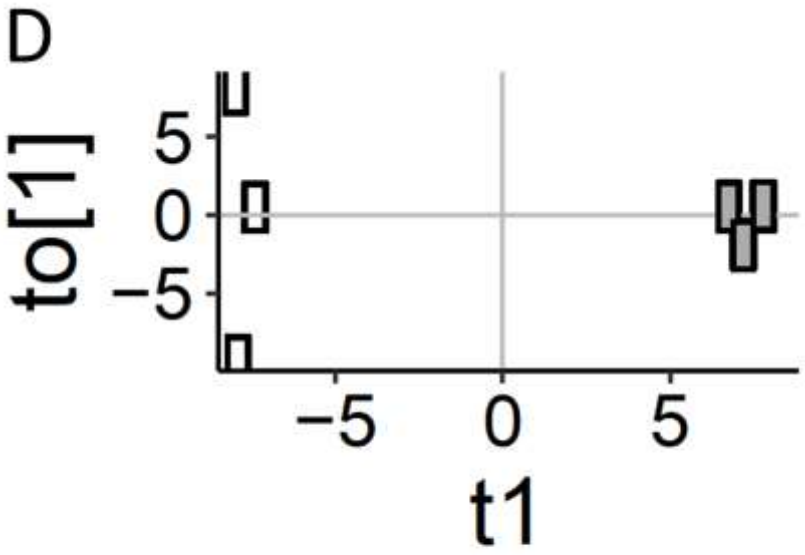
D
to[1]
5
0
−5
−5
0
5
t1

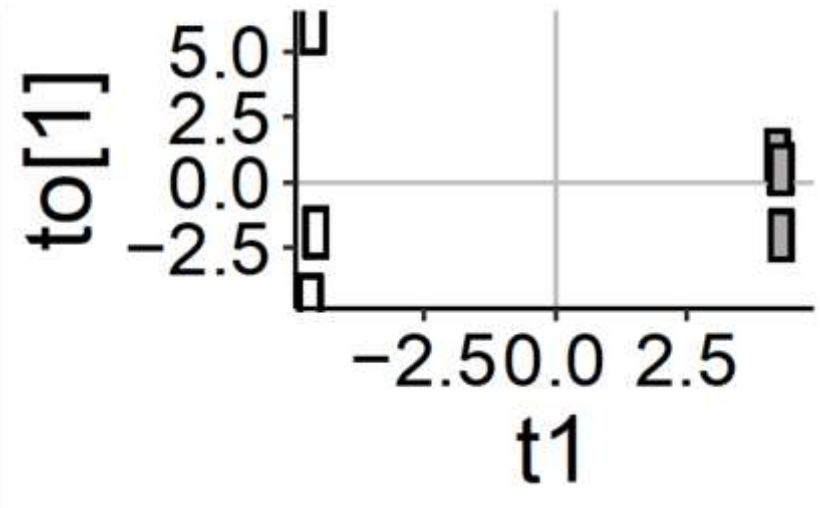
to[1]
5.0
2.5
0.0
−2.5
−2.5
0.0
2.5
t1

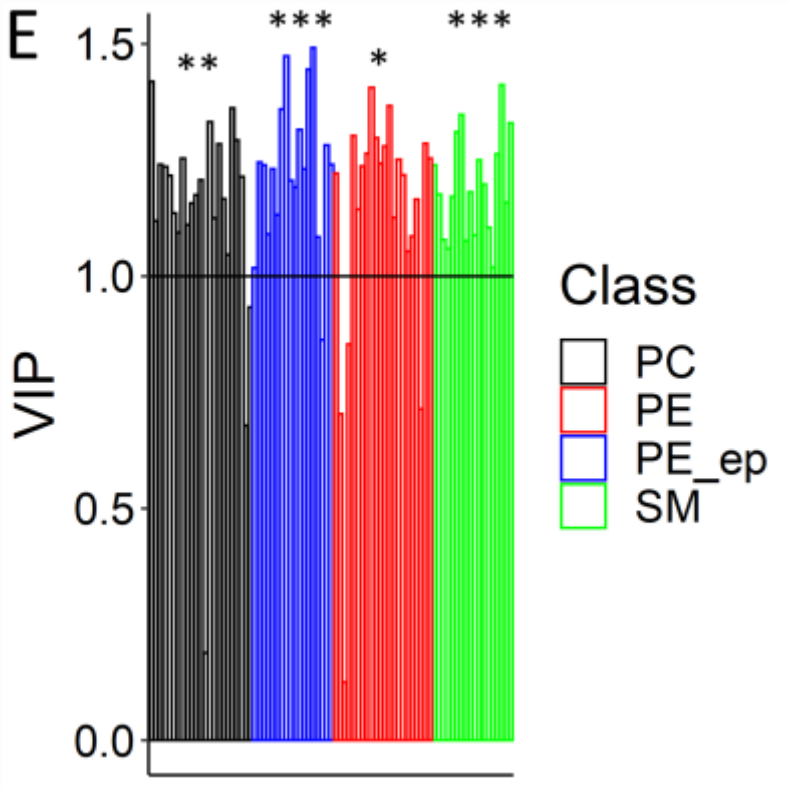

Figure 6. Reduced cholesterol and altered plasma membrane lipid content in EHD2 KO adipocytes

Whole cell (A) and plasma membrane samples (B) were subjected to immunoblotting for Munc18c, Syntaxin 4 (Sx4) and SNAP23. All data are presented as % of WT levels (WT=100%, dashed line), n=3 biological replicates (A) and n=3-6 (B). Data are displayed as mean±SD, and unpaired two-sample t-test was used for statistical analysis. Significance was determined according to **p≤0.01. (C) Cholesterol levels in fat cake (FC), plasma membrane (PM), and serum (S) from WT and EHD2 KO mice. Differences assessed by two-way ANOVA, involving an interaction (x) between genotype (g) and sample (t) with a post hoc Student´s t-test. (D) Score plots from orthogonal projections to latent structures discriminant analysis (OPLS-DA) calculated on membrane lipidomic data acquired in positive (top) and negative (below) electrospray ionization mode. t1, first predictive component ; to[1], first orthogonal component. WT in white, EHD2 in grey. (E) Lipids showing significant differences between WT and EHD2 KO plasmamembranes (variable importance of projection (VIP)>1). Phosphatidylethanolamine (PE), PE ether lipids (PE_ep), phosphatidylcholine (PC), and sphingomyelin (SM). Enrichment was accessed using Chi-squared statistics; PC_ep, q=0.0013, PE, q=0.011, PE_ep, q=0.00081, SM, q=0.00022. Significance was determined according to *p≤0.05, **p≤0.01 and ***p≤0.001, n=3 biological replicates. NKA= Na^+/K^+-ATPase. All displayed results were obtained from inguinal adipocytes 2 weeks of HFD.

Table 1 Summary of Mass spectrometry data of Syntaxin 16 co-immunoprecipitation analysis.

Syntaxin 16 was immunoprecipitated from 3T3-L1 adipocytes incubated in serum-free media for 2h prior to lysis (i.e. in the basal state). Sx16 was immunoprecipitated as outlined and processed for Mass Spec analysis as outlined. Shown are data for EHD2 and mVps45. EHD2 was the most abundant protein identified in this experiment.

Score is the sum of ion scores of all peptides that were identified. Coverage is the percentage of the protein sequence covered by identified peptides. #PSM refers to the number of peptide spectrum matches. # Unique peptides is the number of peptides common to a protein group and which do not occur in the proteins of any other group**.** # Peptides is he total number of distinct peptide sequences identified in the protein group. #PSM is the number of peptide spectrum matches.

Accession #	***Name***	***Score***	***Coverage***	***# Unique peptides***	***# Peptides***	***#PSMs***
IPI00402968.1	EHD2	2285.04	76.98%	41	42	88
IPI00124291.1	mVps45	1230.21	56.32%	34	34	47